Table 1. Immunohistochemical Analysis of Two Types of Invasion in Human Glioblastoma Samples

Case	Age/Sex	Degree of Angiogenesis at the Tumor Border	Degree of Perivascular MAP2e-positive Cell Cuffing	Density of Single Tumor Cell in Cerebral Cortex
1	69/M	+++	+++	+++
2	67/M	+++	+++	+++
3	76/M	++	++	+++
4	58/M	+	+	+++
5	75/M	+	+	+++

that are angiogenesis independent. Recently, temozolomide has been reported as the most effective antiglioma agent; however, not all of the cells in gliomas are destroyed by temozolomide and patient cure has not been achieved. Antiproliferative agents, such as temozolomide, do not have anti-invasive activity, and thus result in treatment failure.

Recent data showing the clinical use of antiangiogenic drugs for recurrent malignant gliomas have been disappointing (37). Some patients treated with bevacizumab, a humanized monoclonal antibody against VEGF, have shown regression of gadolinium-enhancing main tumors, but significant increases in the volume of infiltrative tumor relative to the enhancing tumor were also observed. Similar results have been reported in clinical settings and experimental models (30, 39, 48).

According to our results, most of the malignant glioma originally consisted of both phenotypes of tumor cells. Therefore, these chemotherapies may affect only glioma cells with angiogenesis-dependent invasion and not those with angiogenesis-inde-

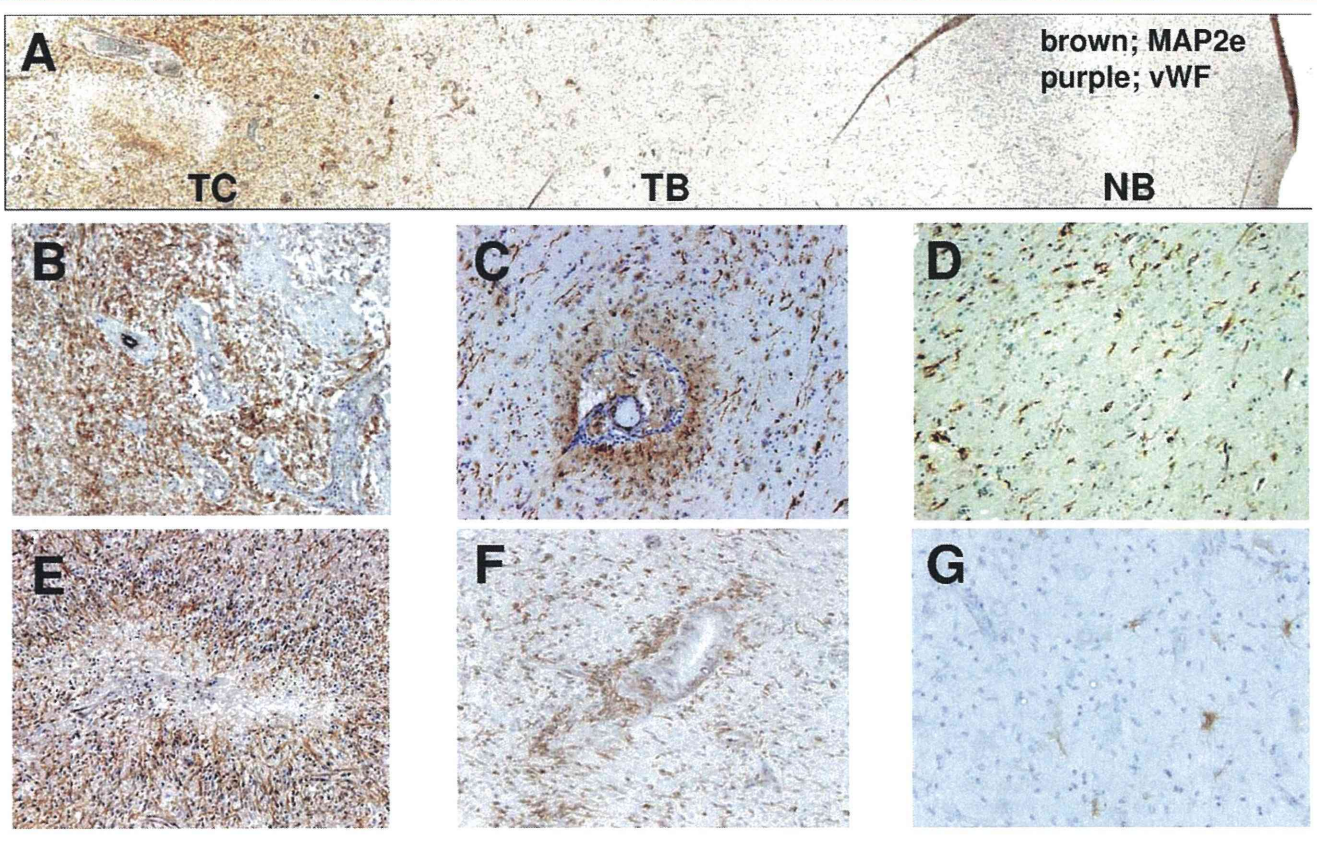

Figure 7. MAP2e and vWf immunohistochemical staining of human glioblastoma samples. Macroscopic appearance of glioblastoma samples in case 2 (**A**). Tumor cells diffusely infiltrated from the tumor center (TC) to the healthy brain (NB) tissue; there is no border between them. TC showed high tumor cell density, endothelial proliferation (**B**, case 3), and pseudopalisading of tumor cells around the necrotic focus (**E**, case 1). At the tumor border (TB), MAP2e-positive tumor cells clustered around dilated vessels (**C**, case 5; **F**, case 1). In NB tissues, single MAP2e-positive tumor cells were diffusely distributed; however, no dilated vessels were observed (**D**, case 1; **G**, case 2). MAP2e, DAB; vWf, DAB-Ni; counterstain, hematoxylin; TC, tumor center; TB, tumor border; NB, healthy brain.

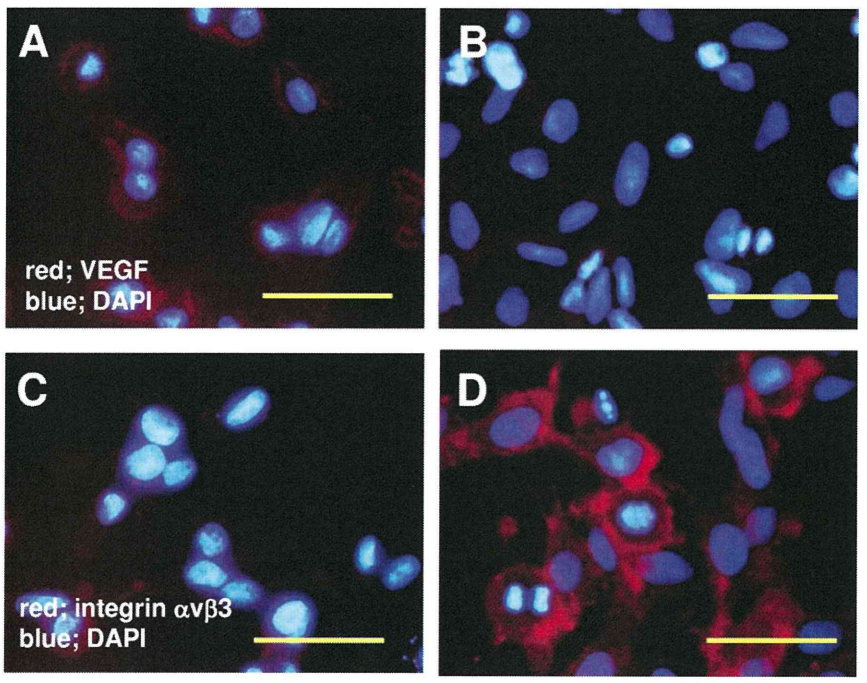

Figure 8. Vascular endothelial growth factor (VEGF) and integrin $\alpha v\beta 3$ immunofluorescent microscopy of J3T-1 and J3T-2 cells. Cultured J3T-1 and J3T-2 cells were stained for VEGF and integrin $\alpha v\beta 3$. J3T-1 cells were positive for VEGF (**A**), whereas J3T-2 cells were negative (**B**). J3T-2 cells were strongly positive for integrin $\alpha v\beta 3$ (**D**) compared with J3T-1 cells (**C**). Scale bar = 2 μm.

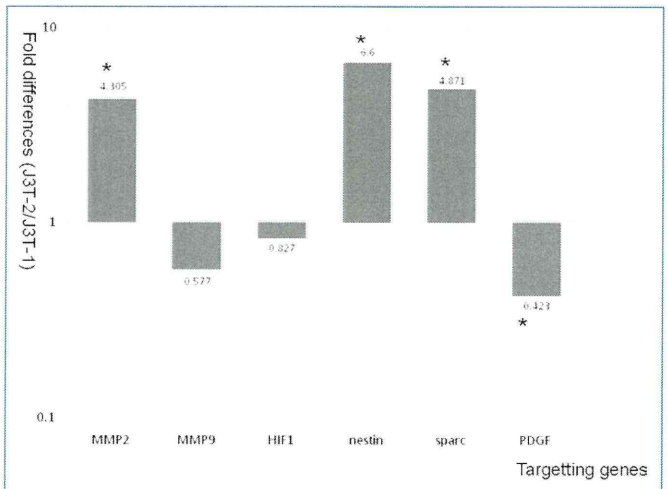

Figure 9. Comparative display of candidate genes of glioma angiogenesis and invasion by quantitative reverse transcription-polymerase chain reaction. Names of transcripts analyzed are on the x-axis and the fold-change increase of each gene in J3T-1 versus J3T-2 (difference in relative copy number, where 1 represents equal expression in both populations) is on the y-axis. Asterisk denotes genes presented more than 1.5-fold change of expression. HIF-1, hypoxia-inducible factor-1; MMP-2, matrix metalloproteinase-2; MMP-9, matrix metalloproteinase-9; sparc, secreted protein acidic and rich in cysteine; PDGF, platelet-derived growth factor.

pendent invasion and may even lead to a switch in the dominant invasion pattern from angiogenesis dependent to angiogenesis independent. As mentioned previously, these distinct invasive patterns complicate curative treatment, and hence, must be distinguished to develop novel approaches for human glioma therapy. Curative treatment of gliomas should target cells with both angiogenesis-dependent and angiogenesis-independent invasion concurrently. Our animal models facilitated their identification, and thereby, the development of novel therapeutic strategies such as oncolytic viruses, tumor-targeted stem cell, or immunotherapy (24, 26, 28, 31).

Usefulness of our Models for Molecular Analysis and Experimental Therapy

J3T-1 and J3T-2 brain tumor models provide a reproducible in vitro and in vivo system to study the mechanisms of invasion and angiogenesis of gliomas. There are several advantages to our novel animal models.

First, J3T-1 and J3T-2 brain tumor models are the exclusive cell line-based invasive animal models. Traditional animal models of glioma have been criticized for not recapitulating the main pathologic features of human glioma (13). They developed a well-demarcated tumor mass at the inoculation site, but did not aggressively invade healthy brain tissue. Recently, some animal models have been reported in which human glioma xenografts showed various degrees of diffuse invasion (10, 14, 16, 17, 21, 25, 50). However, these models required some special procedures to establish brain tumors, such as in vivo preparation of xenografts or in vitro spheroid formation before implantation (10, 20, 34, 50). They cost and need more time than cell line-based animal models. Another disadvantage of these models was that tumors grew slowly, and thus, required a long observation period. Compared with these models, our cell line-based models can be established easily with uncomplicated cell preparations and they have shown stable reproducibility of tumor development as well as the same phenotypic growth shown in human glioma. The moderate survival time of the animals is also suitable for experimental assessment. In addition, there is a potential utility of these cells to establish invasive glioma models in immunocompetent canines. Berens et al. (6) established allogeneic brain tumor

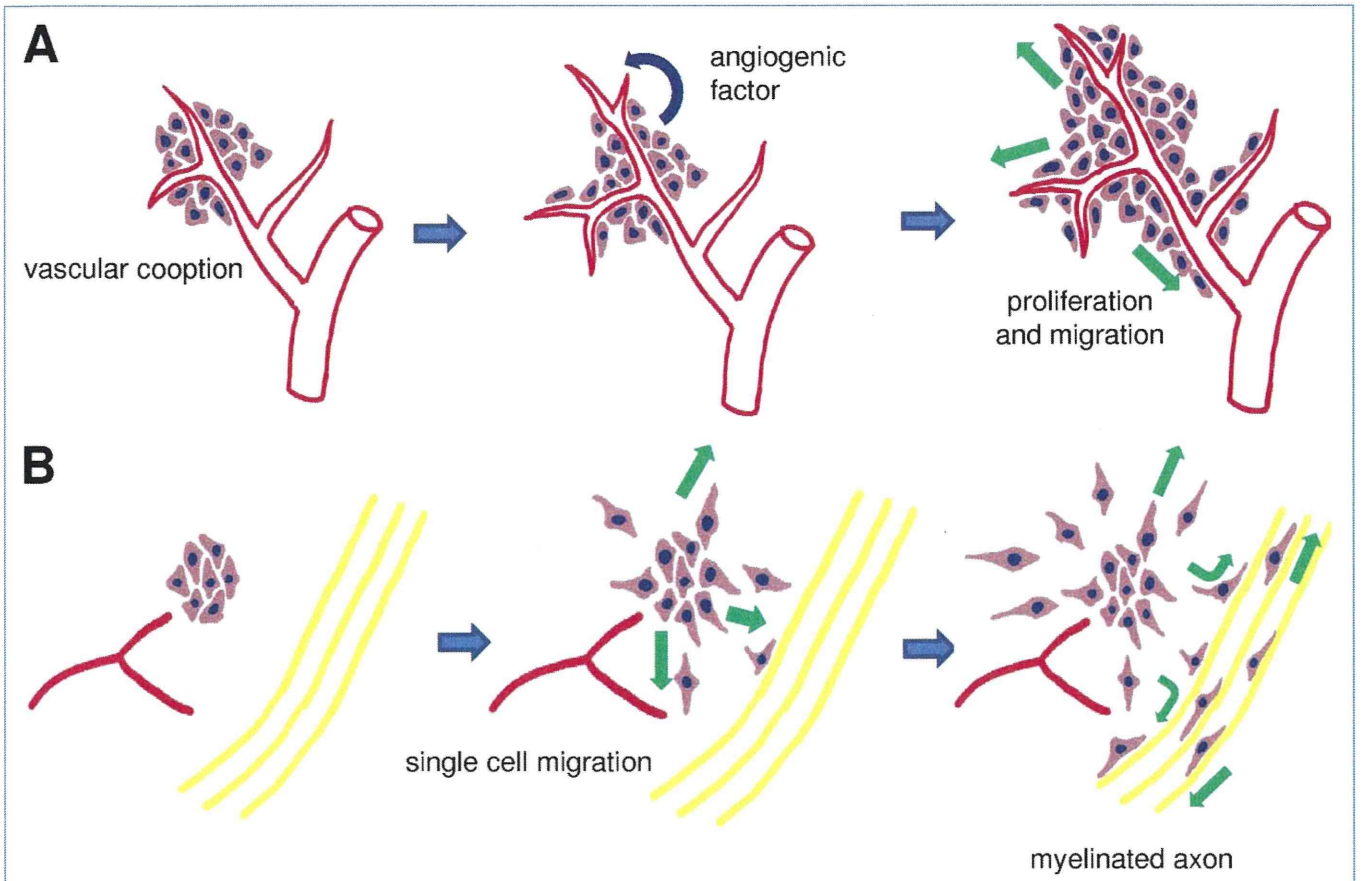

Figure 10. Schematic representation of the two invasion phenotypes. (**A**) Angiogenesis-dependent invasion. Tumor cells coopt around preexisting vessels and secrete angiogenic factors to develop neovasculature. Tumor cells proliferate around newly developed vessels and migrate along them, resulting in the formation of perivascular cuffing. (**B**) Angiogenesis-independent invasion. Tumor cells migrate as single cells along myelinated axons without inducing angiogenesis.

model in immunocompetent canine. Candolfi et al. (8, 9) reported that spontaneous canine glioblastoma very closely approximate the human disease relative to histopathology, epidemiology, and clinical course. Because the canine glioma model is the only large animal model available, this would be more useful for establishing novel therapies to optimize treatment schedule and to assess immune response or therapy-related toxicity.

Second, the most significant advantage of our models is that they are a pair of sibling subclones that show different phenotypes in vivo, but have a similar genetic background. Similarity in genotype but difference in phenotype makes our models suitable for comparative study of genetic or proteomic profiles to narrow down molecular fluctuations between the types in experimental settings. Molecular materials for canine cells are limited; however, some microarrays or antibodies are commercially available. Therefore, our model is suitable for molecular analysis to elucidate the mechanisms of glioma invasion. We have shown molecular profiles of these cell lines that may regulate each phenotypes of invasion by comparative analysis of gene or protein expression between subclones J3T-1 and J3T-2. Furthermore, results of in vitro analysis can be directly verified in vivo using our animal models.

Third, animals harboring J3T-1 or J3T-2 brain tumors die of tumor progression. Therefore, these animal models are suitable for the assessment of experimental treatments. The lack of glioma models that mimic the pathologic condition of human glioma has been responsible, in some part, for the failure of conventional therapy. Models that especially reflect invasive phenotypes are absolutely necessary for the development and evaluation of novel therapeutic approaches.

CONCLUSIONS

In the present study we have established two new cell line-based animal models of invasive glioma. Each of our animal models, J3T-1 and J3T-2, histologically recapitulated two invasive and angiogenic phenotypes, namely angiogenesis-dependent and angiogenesis-independent invasion, also observed in human glioblastoma. Molecular profiles of these cell lines, which may regulate each phenotype of invasion, were shown by comparative analysis of gene or protein expression between two subclones. This unique pair of cell lines provided a reproducible in vitro and in vivo system to analyze the mechanisms of invasion and angiogenesis in glioma progression.

ACKNOWLEDGMENTS

We thank H. Wakimoto, M. Arao, and A. Ishikawa for their technical assistance. The following medical students also contributed animal experiments: T. Oka, K. Tanaka, H. Honda, K. Seno, H. Okura, T. Mifune, and S. Murai.

REFERENCES

1. Barth RF, Kaur B: Rat brain tumor models in experimental neuro-oncology: the c6, 9l, t9, rg2, f98, bt4c, rt-2 and cns-1 gliomas. J Neurooncol 94:299-312, 2009.

2. Beier D, Hau P, Proescholdt M, Lohmeier A, Wischhusen J, Oefner PJ, Aigner L, Brawanski A, Bogdahn U, Beier CP: Cd133(+) and cd133(-) glioblastoma-derived cancer stem cells show differential growth characteristics and molecular profiles. Cancer Res 67:4010-4015, 2007.

3. Bellail AC, Hunter SB, Brat DJ, Tan C, Van Meir EG: Microregional extracellular matrix heterogeneity in brain modulates glioma cell invasion. Int J Biochem Cell Biol 36:1046-1069, 2004.

4. Bello L, Francolini M, Marthyn P, Zhang J, Carroll RS, Nikas DC, Strasser JF, Villani R, Cheresh DA, Black PM: Alpha(v)beta3 and alpha(v)beta5 integrin expression in glioma periphery. Neurosurgery 49: 380-389 [discussion: 390], 2001.

5. Berens ME, Bjotvedt G, Levesque DC, Rief MD, Shapiro JR, Coons SW: Tumorigenic, invasive, karyotypic, and immunocytochemical characteristics of clonal cell lines derived from a spontaneous canine anaplastic astrocytoma. In Vitro Cellular & Developmental Biology-Animal 29:310-318, 1993.

6. Berens ME, Giese A, Shapiro JR, Coons SW: Allogeneic astrocytoma in immune competent dogs. Neoplasia 1:107-112, 1999.

7. Bernsen H, Van der Laak J, Kusters B, Van der Ven A, Wesseling P: Gliomatosis cerebri: quantitative proof of vessel recruitment by cooptation instead of angiogenesis. J Neurosurg 103:702-706, 2005.

8. Candolfi M, Curtin JF, Nichols WS, Muhammad AG, King GD, Pluhar GE, McNiel EA, Ohlfest JR, Freese AB, Moore PF, Lerner J, Lowenstein PR, Castro MG: Intracranial glioblastoma models in preclinical neuro-oncology: neuropathological characterization and tumor progression. J Neurooncol 85: 133-148, 2007.

9. Candolfi M, Pluhar GE, Kroeger K, Puntel M, Curtin J, Barcia C, Muhammad AKM, Xiong W, Liu C, Mondkar S: Optimization of adenoviral vector-mediated transgene expression in the canine brain in vivo, and in canine glioma cells in vitro. Neuro-Oncology 9:245-258, 2007.

10. Claes A, Wesseling P, Jeuken J, Maass C, Heerschap A, Leenders WP: Antiangiogenic compounds interfere with chemotherapy of brain tumors due to vessel normalization. Mol Cancer Ther 7:71-78, 2008.

11. Cretu A, Fotos JS, Little BW, Galileo DS: Human and rat glioma growth, invasion, and vascularization in a novel chick embryo brain tumor model. Clin Exp Metastasis 22:225-236, 2005.

12. Demuth T, Berens ME: Molecular mechanisms of glioma cell migration and invasion. J Neurooncol 70:217-228, 2004.

13. Ding H, Nagy A, Gutmann DH, Guha A: A review of astrocytoma models. Neurosurg Focus 8:1-8, 2000.

14. Engebraaten O, Hjortland GO, Hirschberg H, Fodstad O: Growth of precultured human glioma specimens in nude rat brain. J Neurosurg 90:125-132, 1999.

15. Farin A, Suzuki SO, Weiker M, Goldman JE, Bruce JN, Canoll P: Transplanted glioma cells migrate and proliferate on host brain vasculature: a dynamic analysis. Glia 53:799-808, 2006.

16. Galli R, Binda E, Orfanelli U, Cipelletti B, Gritti A, De Vitis S, Fiocco R, Foroni C, Dimeco F, Vescovi A: Isolation and characterization of tumorigenic, stem-like neural precursors from human glioblastoma. Cancer Res 64:7011-7021, 2004.

17. Giannini C, Sarkaria JN, Saito A, Uhm JH, Galanis E, Carlson BL, Schroeder MA, James CD: Patient tumor egfr and pdgfra gene amplifications retained in an invasive intracranial xenograft model of glioblastoma multiforme. Neuro Oncol 7:164-176, 2005.

18. Giese A, Bjerkvig R, Berens ME, Westphal M: Cost of migration: invasion of malignant gliomas and implications for treatment. J Clin Oncol 21:1624-1636, 2003.

19. Golembieski WA, Rempel SA: Cdna array analysis of sparc-modulated changes in glioma gene expression. J Neurooncol 60:213-226, 2002.

20. Goplen D, Wang J, Enger PO, Tysnes BB, Terzis AJA, Laerum OD, Bjerkvig R: Protein disulfide isomerase expression is related to the invasive properties of malignant glioma. Cancer Res 66:9895-9902, 2006.

21. Gunther HS, Schmidt NO, Phillips HS, Kemming D, Kharbanda S, Soriano R, Modrusan Z, Meissner H, Westphal M, Lamszus K: Glioblastoma-derived stem cell-enriched cultures form distinct subgroups according to molecular and phenotypic criteria. Oncogene 27:2897-2909, 2008.

22. Hampl JA, Camp SM, Mydlarz WK, Hampl M, Ichikawa T, Chiocca EA, Louis DN, Sena-Esteves M, Breakefield XO: Potentiated gene delivery to tumors using herpes simplex virus/epstein-barr virus/rv tribrid amplicon vectors. Hum Gene Ther 14:611-626, 2003.

23. Holash J, Maisonpierre PC, Compton D, Boland P, Alexander CR, Zagzag D, Yancopoulos GD, Wiegand SJ: Vessel cooption, regression, and growth in tumors mediated by angiopoietins and vegf. Science 284:1994, 1999.

24. Hong X, Miller C, Savant-Bhonsale S, Kalkanis SN: Antitumor treatment using interleukin-12-secreting marrow stromal cells in an invasive glioma model. Neurosurgery 64:1139-1146 [discussion: 1146-1137], 2009.

25. Horten BC, Basler GA, Shapiro WR: Xenograft of human malignant glial tumors into brains of nude mice. A histopatholgical study. J Neuropathol Exp Neurol 40:493-511, 1981.

26. Ichikawa T, Chiocca EA: Comparative analyses of transgene delivery and expression in tumors inoculated with a replication-conditional or -defective viral vector. Cancer Res 61:5336-5339, 2001.

27. Ichikawa T, Tamiya T, Adachi Y, Ono Y, Matsumoto K, Furuta T, Yoshida Y, Hamada H, Ohmoto T: In vivo efficacy and toxicity of 5-fluorocytosine/cytosine deaminase gene therapy for malignant gliomas mediated by adenovirus. Cancer Gene Ther 7:74-82, 2000.

28. Kambara H, Okano H, Chiocca EA, Saeki Y: An oncolytic hsv-1 mutant expressing icp34.5 under control of a nestin promoter increases survival of animals even when symptomatic from a brain tumor. Cancer Res 65:2832-2839, 2005.

29. Kitai R, Horita R, Sato K, Yoshida K, Arishima H, Higashino Y, Hashimoto N, Takeuchi H, Kubota T, Kikuta K: Nestin expression in astrocytic tumors delineates tumor infiltration. Brain Tumor Pathol 27:17-21, 2010.

30. Kunkel P, Ulbricht U, Bohlen P, Brockmann MA, Fillbrandt R, Stavrou D, Westphal M, Lamszus K: Inhibition of glioma angiogenesis and growth in vivo by systemic treatment with a monoclonal antibody against vascular endothelial growth factor receptor-2. Cancer Res 61:6624-6628, 2001.

31. Kurozumi K, Hardcastle J, Thakur R, Yang M, Christoforidis G, Fulci G, Hochberg FH, Weissleder R, Carson W, Chiocca EA, Kaur B: Effect of tumor microenvironment modulation on the efficacy of oncolytic virus therapy. J Natl Cancer Inst 99:1768-1781, 2007.

32. Lakka SS, Gondi CS, Yanamandra N, Olivero WC, Dinh DH, Gujrati M, Rao JS: Inhibition of cathepsin b and mmp-9 gene expression in glioblastoma cell line via RNA interference reduces tumor cell invasion, tumor growth and angiogenesis. Oncogene 23:4681-4689, 2004.

33. Louis DN, Ohgaki H, Wiestler OD, Cavenee WK, Burger PC, Jouvet A, Scheithauer BW, Kleihues P: Glioblastoma. In: WHO Classification of Tumours of the Central Nervous System. vol 2. Lyon: IARC; 2007:33-49.

34. Mahesparan R, Read TA, Lund-Johansen M, Skaftnesmo K, Bjerkvig R, Engebraaten O: Expression of extracellular matrix components in a highly infiltrative in vivo glioma model. Acta Neuropathologica 105:49-57, 2003.

35. Martens T, Laabs Y, Gunther HS, Kemming D, Zhu Z, Witte L, Hagel C, Westphal M, Lamszus K: Inhibition of glioblastoma growth in a highly invasive nude mouse model can be achieved by targeting epidermal growth factor receptor but not vascular endothelial growth factor receptor-2. Clin Cancer Res 14:5447-5458, 2008.

36. Mentlein R, Held-Feindt J: Angiogenesis factors in gliomas: a new key to tumour therapy? Naturwissenschaften 90:385-394, 2003.

37. Norden AD, Young GS, Setayesh K, Muzikansky A, Klufas R, Ross GL, Ciampa AS, Ebbeling LG, Levy B, Drappatz J: Bevacizumab for recurrent malignant gliomas: efficacy, toxicity, and patterns of recurrence. Neurology 70:779-787, 2008.

38. Raithatha SA, Muzik H, Muzik H, Rewcastle NB, Johnston RN, Edwards DR, Forsyth PA: Localization of gelatinase-a and gelatinase-b mRNA and protein in human gliomas. Neuro Oncol 2:145-150, 2000.

39. Rubenstein JL, Kim J, Ozawa T, Zhang M, Westphal M, Deen DF, Shuman MA: Anti-vegf antibody treatment of glioblastoma prolongs survival but results in increased vascular cooption. Neoplasia 2:306-314, 2000.

40. Sakariassen PO, Prestegarden L, Wang J, Skaftnesmo KO, Mahesparan R, Molthoff C, Sminia P, Sundlisaeter E, Misra A, Tysnes BB, Chekenya M, Peters H, Lende G, Kalland KH, Oyan AM, Petersen K, Jonassen I, van der Kogel A, Feuerstein BG, Terzis AJ, Bjerkvig R, Enger PO: Angiogenesis-independent tumor growth mediated by stem-like cancer cells. Proc Natl Acad Sci U S A 103:16466-16471, 2006.

41. Scherer HJ: The forms of growth in gliomas and the practical significance. Brain 63:1-35, 1940.

42. Schultz C, Lemke N, Ge S, Golembieski WA, Rempel SA: Secreted protein acidic and rich in cysteine promotes glioma invasion and delays tumor growth in vivo. Cancer Res 62:6270-6277, 2002.

43. Stupp R, Hegi ME, Mason WP, van den Bent MJ, Taphoorn MJ, Janzer RC, Ludwin SK, Allgeier A, Fisher B, Belanger K, Hau P, Brandes AA, Gijtenbeek J, Marosi C, Vecht CJ, Mokhtari K, Wesseling P, Villa S, Eisenhauer E, Gorlia T, Weller M, Lacombe D, Cairncross JG, Mirimanoff RO: Effects of radiotherapy with concomitant and adjuvant temozolomide versus radiotherapy alone on survival in glioblastoma in a randomised phase III study: 5-year analysis of the EORTC-NCIC trial. Lancet Oncol 10:459-466, 2009.

44. Suzuki SO, Kitai R, Llena J, Lee SC, Goldman JE, Shafit-Zagardo B: Map-2e, a novel map-2 isoform, is expressed in gliomas and delineates tumor architecture and patterns of infiltration. J Neuropathol Exper Neurol 61:403-412, 2002.

45. Takano S, Yamashita T, Ohneda O: Molecular therapeutic targets for glioma angiogenesis. J Oncol 2010:351908, 2010.

46. Tate MC, Aghi MK: Biology of angiogenesis and invasion in glioma. Neurotherapeutics 6:447-457, 2009.

47. Tovi M, Hartman M, Lilja A, Ericsson A: MR imaging in cerebral gliomas. Tissue component analysis in correlation with histopathology of whole-brain specimens. Acta Radiol 35:495-505, 1994.

48. Tuettenberg J, Friedel C, Vajkoczy P: Angiogenesis in malignant glioma? A target for antitumor therapy? Crit Rev Oncol Hematol 59:181-193, 2006.

49. Tysnes BB, Mahesparan R: Biological mechanisms of glioma invasion and potential therapeutic targets. J Neurooncol 53:129-147, 2001.

50. Wang J, Miletic H, Sakariassen PO, Huszthy PC, Jacobsen H, Brekka N, Li X, Zhao P, Mork S, Chekenya M, Bjerkvig R, Enger PO: A reproducible brain tumour model established from human glioblastoma biopsies. BMC Cancer 9:465, 2009.

Conflict of interest statement: This study was supported by grants-in-aid for Scientific Research from the Japanese Ministry of Education, Culture, Sports, Science, and Technology to Tomotsugu Ichikawa (19591675), Hirokazu Kambara (19591676), and Kazuhiko Kurozumi (20890133 and 21791364).

received 28 February 2011; accepted 02 September 2011

Citation: World Neurosurg. (2011) xx, x:xxx.
DOI: 10.1016/j.wneu.2011.09.005

Journal homepage: www.WORLDNEUROSURGERY.org

Available online: ***www.sciencedirect.com***

1878-8750/$ - see front matter *© 2011 Elsevier Inc. All rights reserved.*

Transdifferentiation of glioblastoma cells into vascular endothelial cells

Yasushi Soda[a], Tomotoshi Marumoto[a,b], Dinorah Friedmann-Morvinski[a], Mie Soda[a], Fei Liu[a], Hiroyuki Michiue[c], Sandra Pastorino[d], Meng Yang[e], Robert M. Hoffman[e,f], Santosh Kesari[d], and Inder M. Verma[a,1]

[a]Laboratory of Genetics, Salk Institute for Biological Studies, La Jolla, CA 92037; [b]Division of Molecular and Clinical Genetics, Department of Molecular Genetics, Medical Institute of Bioregulation, Kyushu University, Higashi-ku, Fukuoka 812-8582, Japan; [c]Department of Physiology, Okayama University Graduate School of Medicine, Dentistry, and Pharmaceutical Sciences, Okayama 700-8558, Japan; [d]Department of Neurosciences, Moore's Cancer Center, University of California at San Diego, La Jolla, CA 92093; [e]AntiCancer, Inc., San Diego, CA 92111; and [f]Department of Surgery, University of California at San Diego, San Diego, CA 92103

This Feature Article is part of a series identified by the Editorial Board as reporting findings of exceptional significance.

Edited by Douglas Hanahan, Swiss Institute for Experimental Cancer Research and Swiss Federal Institute of Technology Lausanne, Lausanne, Switzerland, and approved December 27, 2010 (received for review October 26, 2010)

Glioblastoma (GBM) is the most malignant brain tumor and is highly resistant to intensive combination therapies and anti-VEGF therapies. To assess the resistance mechanism to anti-VEGF therapy, we examined the vessels of GBMs in tumors that were induced by the transduction of $p53^{+/-}$ heterozygous mice with lentiviral vectors containing oncogenes and the marker GFP in the hippocampus of GFAP-Cre recombinase (Cre) mice. We were surprised to observe GFP^+ vascular endothelial cells (ECs). Transplantation of mouse GBM cells revealed that the tumor-derived endothelial cells (TDECs) originated from tumor-initiating cells and did not result from cell fusion of ECs and tumor cells. An in vitro differentiation assay suggested that hypoxia is an important factor in the differentiation of tumor cells to ECs and is independent of VEGF. TDEC formation was not only resistant to an anti-VEGF receptor inhibitor in mouse GBMs but it led to an increase in their frequency. A xenograft model of human GBM spheres from clinical specimens and direct clinical samples from patients with GBM also showed the presence of TDECs. We suggest that the TDEC is an important player in the resistance to anti-VEGF therapy, and hence a potential target for GBM therapy.

mouse model | glioma | angiogenesis | hypoxia-inducible factor 1

Glioblastoma multiforme (GBM) is the most common and lethal form of brain cancer. Despite optimal treatment and evolving standard of care, the median survival of patients diagnosed with GBM is only 12–15 mo (1). Because GBM is one of the most vascular-rich tumors and VEGF is produced by tumor cells, the anti-VEGF antibody bevacizumab (Avastin) is being used in clinical trials (2). In a phase II clinical trial, more than half of the patients with GBM responded to the combination treatment of bevacizumab and irinotecan, but this effect was transient in most patients (3). Mechanisms proposed to explain resistance to anti-VEGF therapy include activation of other proangiogenic signaling pathways, recruitment of bone marrow (BM)-derived myeloid cells that protect and nurture vascular cells, protection of blood vessels by increased pericyte coverage, and increased tumor invasion (4, 5). In GBMs, the antitumor effect of the antiangiogenic therapies is likely attributable to normalization of vasculature, which also decreases edema (3, 6). Recent studies have shown that tumor cells become more aggressive after antiangiogenic therapy (7).

The tumor vessels in GBMs are different from normal blood vessels morphologically and functionally. As with other tumors, the tumor vessels in GBMs are tortuous; disorganized; highly permeable; and abnormal in the endothelial walls, pericyte coverage, and basement membrane, resulting in loss of the blood–brain barrier (2). In addition, angiogenesis in GBMs has a unique feature, so-called "glomeruloid tufts," exhibiting aggressive proliferation of endothelial cells (ECs) compared with those of anaplastic glioma (grade III) (2). Recently, the possibility of EC differentiation of tumor cells has been suggested in lymphoma, myeloma, chronic myeloid leukemia (CML), breast cancer, and neuroblastoma (8–12). Therefore, we surmised that the mechanism of vascular formation in GBM may also be different from that of regular tumor vascular formation.

To investigate angiogenesis in GBMs, we examined our recent mouse GBM model in which tumors developed 2–6 mo after injection with viral vectors. The tumors showed all the features of GBM, including hypervascularity (13). Furthermore, tumors were GFP^+, because the vectors contained GFP in addition to activated oncogenes and loss of p53. Interestingly, in these tumors, we found many GFP^+ cells with EC characteristics, particularly in the deep area of the lesions, by confocal microscopy and flow cytometry, indicating the presence of tumor-derived endothelial cells (TDECs). Here, we demonstrate that the TDECs originated from tumor-initiating cells but not from contaminated EC progenitors or cell-to-cell fusion between tumor cells and ECs. The TDECs are functional because blood flows through them. Additionally, it has been suggested that hypoxia-inducible factor 1 (HIF-1) is an important enhancer of EC differentiation of tumor cells and that the formation of TDECs is independent of VEGF. Finally, direct clinical samples from patients show EC cells with tumor markers. Our report shows direct evidence of TDEC formation in GBMs, which may play a role in the resistance to anti-VEGF therapy.

Results

ECs Express Tumor-Specific Marker in Mouse GBM Models. To investigate angiogenesis in GBMs, we used our recent mouse GBM model (13). As previously reported, Cre recombinase (Cre)-loxP–controlled lentiviral vectors encoding the activated form of oncogenes H-Ras and Akt [pTomo vectors (13)] were injected stereotaxically into the hippocampus of GFAP-Cre-$p53^{+/-}$ mice. In this model, the oncogenes were expressed specifically in $GFAP^+$ cells and tumors expressed GFP, H-Ras, and Akt and showed loss of p53. Additionally, they were positive for the neural progenitor cell marker nestin, which is often expressed in human GBMs (14). To investigate the tumor vasculature, we carried out immunofluorescence by confocal microscopy using the endothelial antigens von Willebrand factor (vWF), CD31, CD34, and vascular endothelium (VE)-cadherin (CD144) as markers. Fig. 1*A* shows a normal EC, where the GFP

Author contributions: Y.S. and I.M.V. designed research; Y.S., T.M., D.F.-M., M.S., F.L., and H.M. performed research; S.P., M.Y., R.M.H., and S.K. contributed new reagents/analytic tools; Y.S., D.F.-M., and I.M.V. analyzed data; and Y.S., D.F.-M., S.K., and I.M.V. wrote paper.

The authors declare no conflict of interest.

This article is a PNAS Direct Submission.

See Commentary on page 4271.

[1]To whom correspondence should be addressed. E-mail: verma@salk.edu.

This article contains supporting information online at www.pnas.org/lookup/suppl/doi:10.1073/pnas.1016030108/-/DCSupplemental.

in tumor cells is completely distinct from vWF, the endothelial antigen (Fig. 1*A*, *i–iii*). Surprisingly, we found that some ECs expressed not only endothelial antigens but also GFP, which most likely originated from tumor cells (Fig. 1*B*, *i–iii*, compare with the merge in Fig. 1 *A*, *iii*, and *B*, *iii*, and Fig. S1*A*). Additionally some GFP$^+$ ECs formed vessels with GFP$^-$ regular ECs, exhibiting a mosaic pattern [Fig. 1*B*, *iv–vi*; a *z*-series assay further confirmed the mosaic pattern (Fig. S1*A*)]. Immunofluorescence with other EC-specific antigens like CD34 and CD144 also showed EC cells containing GFP, further supporting the formation of TDECs (Fig. *1B*, *vii–xii*). The GFP$^+$ ECs expressed the transduced oncogene Flag-tagged H-RasV12 (Fig. 1*C*, *i–v*). Similar results were obtained with HA-tagged Akt. Nestin expressed in tumor cells can be detected in both GFP$^+$ EC cells (marked T) and GFP$^-$ EC cells (marked R), further strengthening the notion that GFP$^+$ ECs (TDECs) most likely originated from the tumor cells (Fig. 1*C* *vi–x*). The TDECs were also observed when GBM was generated using lentivectors (LVs) containing only activated H-Ras and small interfering p53 (sip53). To confirm the presence of GFP$^+$ ECs, we also examined dissociated tumors by flow cytometry. Similar to the results of confocal microscopy, 10–25% of ECs (CD45$^-$CD31$^+$CD34$^+$) were positive for GFP (Fig. 1*D*). The TDECs were mostly found in the deep part of the tumor rather than on its surface, and the frequency of vessels containing the GFP$^+$ ECs was 6.4–37.8% (average of 24.6 ± 12.7%) in the deep area, depending on the size of the tumor. In the surface area, 2.0–12.7% (average of 8.33 ± 4.15%) of vessels contained the GFP$^+$ ECs (Table S1). In general, the frequency of the TDECs was higher in large tumors than in smaller tumors. By injecting Hypoxyprobe-1 (Natural Pharmacia International) into tail veins of tumor-harboring mice, we showed that the deep area of the tumor was more hypoxic than the surface area (Fig. 2*A*), suggesting that hypoxia may be an important factor for TDEC formation. Hypoxia leads to angiogenesis by induction of VEGF through increasing levels of HIF-1. Furthermore, tumors produced VEGF (13, 15). We are now pursuing HIF-1 expression by immunofluorescence studies. Interestingly, the majority of TDECs did not express VEGF receptor 2 (R2) (Fig. 2*B*, *vi–x*), whereas most of the regular ECs (GFP$^-$) expressed VEGF-R2 (Fig. 2*B*, *i–v*). The TDECs also did not show expression of VEGF-R1 and VEGF-R3. Because FGF-2 is another important growth factor expressed by the ECs and the GBM cells, we also examined the expression of FGF receptor 1 (FGFR-1). In contrast to the results of VEGF receptors, the FGFR-1 was expressed in both TDECs (marked T) and regular ECs (marked R) as well as in surrounding tumor cells (Fig. 2*C*).

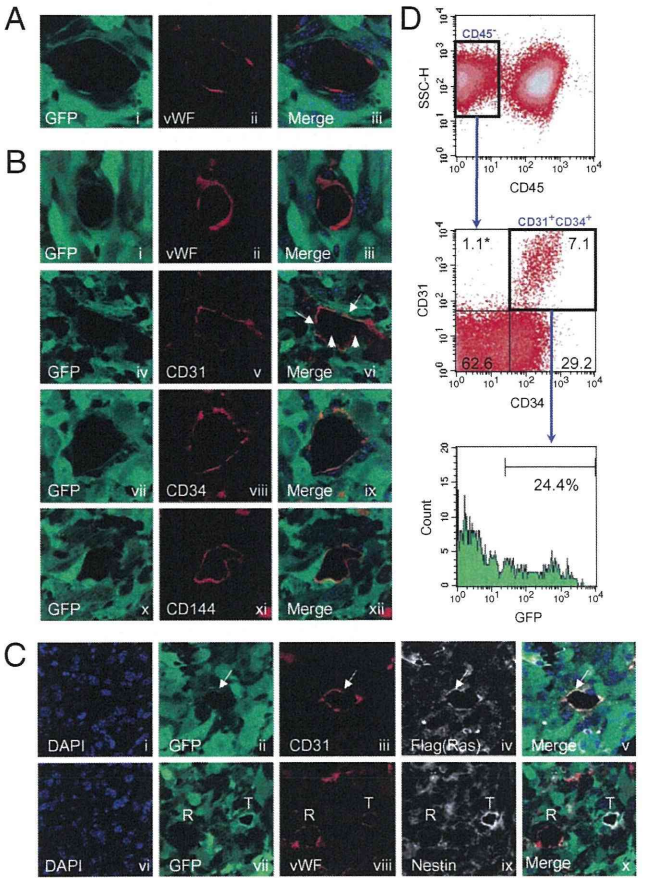

Fig. 1. TDECs. GFAP-Cre/p53$^{+/-}$ mouse brain was transduced by Tomo H-RasV12 LVs and Tomo Akt LVs as described (13). A representative image of ECs observed by confocal microscopy is shown. (*A*) Regular ECs lined the vessel lumen and expressed EC marker vWF (*ii*) but not the tumor marker GFP (*i*). DAPI was used as the nuclear marker, and the image was incorporated in the merge panel (*iii*). (*B*) In contrast, TDECs expressed both the GFP marker (*i*, *iv*, *vii*, and *x*) and EC markers vWF (*ii*), CD31 (*v*), CD34 (*viii*), and CD144 (*xi*). Some GFP$^+$ ECs formed vessels with GFP$^-$ regular ECs (*vi*, arrowheads). DAPI was used as the nuclear marker, and the image was incorporated in the merge panels (*iii*, *vi*, *ix*, and *xii*). (*C*) TDECs expressed Flag-tagged H-RasV12 in addition to GFP and CD31 (*i–v*, arrows). They also expressed nestin in addition to GFP and vWF (*vi–x*, R and T indicate regular ECs and TDECs, respectively). (*D*) Representative result of flow cytometry for dissociated brain tumors. In the CD45$^-$ population (*Top*), ECs were CD31$^+$CD34$^+$ and constituted 7.1% of the whole tumor (*Middle*) and GFP$^+$ ECs (TDECs) represented 24.4% of total ECs (*Bottom*). The asterisk represents the percentage of cells in each quadrant. All confocal pictures are single-slice images at an Airy factor of 1.0. [Magnification: all confocal images were taken at 63× with 3× (*A* and *B*) or 2× (*C*) electrical zoom (total magnification: 189× or 126×).]

TDEC-Forming Vessels Are Functional. To assess if TDECs are functional, we determined blood flow in TDEC-containing vessels. We injected biotinylated lectin i.v., which can bind to ECs in mice harboring brain tumors, 15 min before euthanasia. To

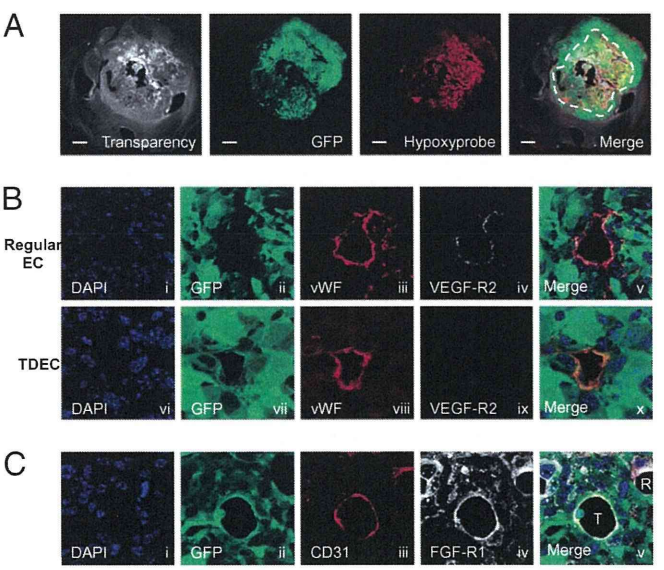

Fig. 2. Hypoxia and expression of HIF-1α and receptors of angiogenic growth factors. (*A*) Hypoxyprobe assay of the tumor. The hypoxic area (pO_2 < 10 mmHg) was detected by the anti-Hypoxyprobe antibody. The dotted line shows the approximate border of the hypoxic area. (Scale bar: 1 mm.) (*B*) Regular tumor ECs expressed VEGF-R2 (*i–v*), but GFP$^+$ TDECs did not express VEGF-R2 (*vi–x*). (*C*) GFP$^+$ TDECs (T) expressed FGF-R1, as did regular ECs (R) and surrounding tumor cells. All confocal pictures are single-slice images at an Airy factor of 1.0. [Magnification: 63× with 3× electrical zoom (total magnification: 189×) except *A*, which was 1.25×.]

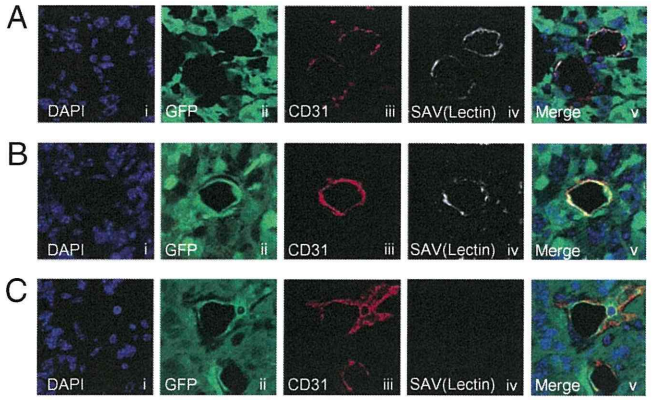

Fig. 3. Blood flow in TDEC-forming vessels. Biotinylated lectin injection assay showed that both regular vessels (*A*) and TDEC-forming vessels (*B*) are functional and allowed blood flow. (*C*) Nonfunctional TDEC-forming vessels were also observed. All confocal pictures are single-slice images at an Airy factor of 1.0. [Magnification: 63× with 3× electrical zoom (total magnification: 189×).]

visualize the blood flow, tumor sections were stained with fluorescence-labeled streptavidin, which binds to biotinylated lectin-labeled ECs. Just like regular ECs, lectin-bound TDECs were observed in many tumors, indicating that the TDEC-forming vessels are functional (Fig. 3 *A* and *B*). There were also nonfunctional TDEC-forming vessels (Fig. 3*C*).

TDECs in Transplanted Tumors. We next investigated the ability of tumor cells to differentiate into ECs by transplanting mouse GBM cell line 005, which is a tumor-initiating cell line established from our lentiviral vector-induced tumor model, into the brain of a nonobese diabetic (NOD)-SCID mouse. On examination of the tumor vessels in the transplanted mice, GFP^+ ECs were observed (Fig. 4*A*, *i–iv*). We further established 14 subclones of the 005 cells and transplanted them into NOD-SCID mouse brains. Most clones formed tumors in the same way as the parental 005 cells and contained GFP^+ ECs in these tumors. Data from one such subclone are shown using CD34 as a marker of ECs (Fig. 4*B*, *i–iv*). Because it has been reported that some $GFAP^+$ neural stem cells (NSCs) can transdifferentiate into ECs (16), it is possible that 005 cells may contain transduced $GFAP^+$ NSCs in addition to tumor-initiating cells and that these $GFAP^+$ NSCs differentiate into the GFP^+ ECs. We therefore generated a cell line from another tumor (006) induced by pTomo vector. Results from 006 cells also show GFP^+ ECs (Fig. 4*C*, *i–iv*), thus minimizing the possibility of the presence of $GFAP^+$ NSCs in tumor-initiating cells that differentiated into the ECs.

Fusion-Independent Mechanism in TDEC Formation. To exclude the possibility that GFP^+ ECs (TDECs) result from cell fusion of tumor cells and ECs but are not derived from tumor cells, we transplanted 005 tumor cells into the brains of DsRed-transgenic nude mice and examined the expression of GFP, DsRed, and EC markers in the transplanted tumors. In these transgenic mice, the DsRed is driven by the CAG promoter and all cell types except hair and red blood cells express DsRed (17). In tumors developed in these mice, many $DsRed^+$ host cells, including ECs, were infiltrating into the tumors (Fig. S1*B*). Confocal microscopy revealed that GFP^- ECs were expressing DsRed (Fig. 4*D*, *i–iv*), whereas GFP^+ ECs were not expressing DsRed (Fig. 4*D*, *v–viii*), thus confirming that the GFP^+ TDECs were derived from a fusion-independent mechanism. To confirm these results, we also examined dissociated tumors by flow cytometry. Similar to the results of confocal microscopy, most of the GFP^+ ECs were $DsRed^-$, whereas $DsRed^+$ ECs were GFP^- (Fig. 4*E*). We further examined the cell fusion in the NOD-SCID mouse transplantation model by flow cytometry. In this model, MHC class I $H\text{-}2K^d$ is expressed in the host cells but not in 005-derived tumor cells.

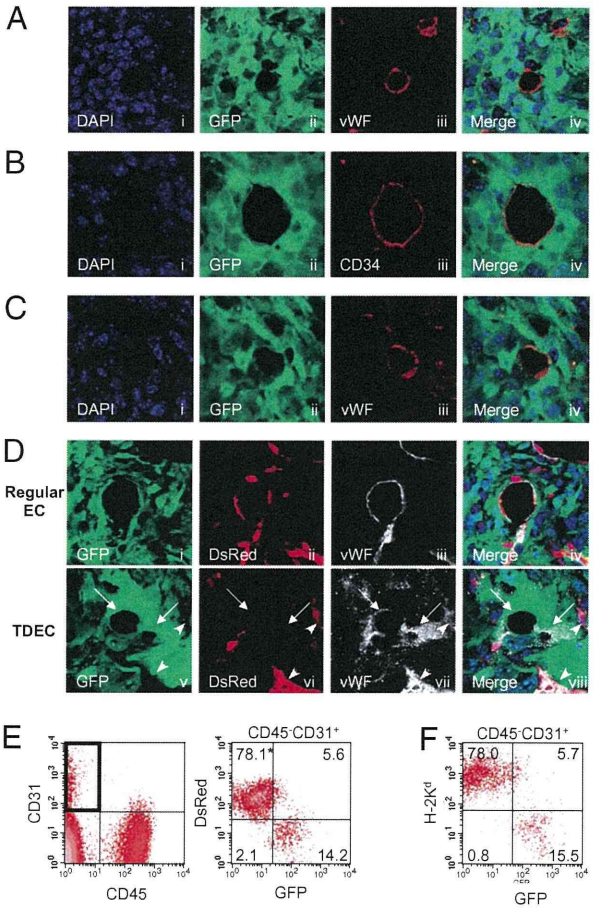

Fig. 4. TDECs in tumor-initiating cells transplanted into immunocompromised mice. Representative images of TDECs in brain tumors developed in NOD-SCID mice transplanted with tumor-initiating cell line. Cell line 005 (*A*), 005 subclone cells (*B*), and another tumor-initiating cell line 006 (*C*). TDECs expressed GFP and EC markers vWF and CD34. (*D*) Representative image of regular ECs and TDECs in brain tumors developed in DsRed nude mice transplanted with 005 cells by confocal microscopy. Regular tumor vessel ECs expressed vWF and host marker DsRed but not tumor marker GFP (*i–iv*), whereas GFP^+ vWF^+ TDECs did not express DsRed (*v–viii*). TDECs are indicated by arrows, and regular ECs are indicated by arrowheads (*v–viii*). All confocal pictures are single-slice images at an Airy factor of 1.0. [Magnification: 63× with 3× electrical zoom (total magnification: 189×).] (*E*) Representative results of flow cytometry of dissociated tumors developed in DsRed nude mice transplanted with 005 subclone cells. In the $CD45^-CD31^+$ EC fraction (*Left*), DsRed-positive cells did not express GFP (*Right*). (*F*) Representative results of flow cytometry for dissociated tumors developed in NOD-SCID mice. In the $CD45^-CD31^+$ EC fraction, cells expressing NOD-SCID mouse-specific $H\text{-}2K^d$ did not express GFP. The asterisk represents the percentage of cells in each quadrant.

The majority of $H\text{-}2K^{d+}$ host-derived ECs were GFP^-, whereas GFP^+ ECs were $H\text{-}2Kd^-$ (Fig. 4*F*), again suggesting a fusion-independent mechanism of TDEC formation.

In Vitro Differentiation of GBM Cells to ECs: Role of Hypoxia and HIF-1. We next attempted to induce GBM initiating cells (005 cells) to differentiate into ECs in vitro. Because HIF-1 is likely to be an important factor for TDEC formation, we added an iron chelator, deferoxamine (DFO), into the culture media to mimic hypoxic conditions by blocking proline hydroxylase (18, 19), which stabilizes HIF-1α. Culturing 005 cells in DMEM/F-12 medium supplemented with FBS (DFS) and endothelial cell growth medium (EGM; Lonza), which contains FBS, human VEGF, human EGF, human FGF-2, insulin-like growth factor, cortisol, and heparin, induced significant morphological changes. DFO en-

hanced the change to endothelial-like morphology in DFS medium or EGM but not in N2 medium, which is used to maintain the NSCs (Fig. 5*A*). In the DFS medium and EGM, DFO significantly enhanced the HIF-1α expression in the 005 cells (Fig. 5*B*) and induced expression of endothelial antigens vWF and CD31 (Fig. 5 *C* and *D*). However, VEGF-R2 expression was induced only in a small population of cells (Fig. 5*D*). Additionally, these differentiated cells formed a tube structure on Matrigel (Becton Dickinson) (Fig. 5*E*). To confirm that this endothelial differentiation results from HIF-1α accumulation but not from a nonspecific effect of DFO, we cultured the 005 cells in 2% O_2 (hypoxia). Tubular structures could be observed in the absence of DFO when these cells were cultured in DFS medium or EGM but not in N2 medium (Fig. 5*E*), suggesting that hypoxia, presumably through the activation of HIF-1 α (Fig. 5*B*), is playing an important role in the endothelial differentiation.

VEGF-Independent Transdifferentiation of Tumor Cells. Because VEGF is a critical factor in tumor angiogenesis and is induced by hypoxia through accumulation of HIF-1α (15), we investigated the role of VEGF in the formation of TDECs. VEGF was released constitutively from 005 cells in N2 medium at a low level (32.2 ± 8.8 pg/mL per 10^6 cells), and the amount of VEGF release increased about threefold in DFS medium and EGM. In the presence of DFO, however, secretion of VEGF in both DFS medium (243 ± 22.2 pg/mL) and EGM (368 ± 32.6 pg/mL) was significantly increased. No effect was observed in N2 medium (Fig. 6*A*). These results suggest that VEGF may play a role in endothelial differentiation of 005 cells. We therefore blocked autocrine VEGF function with anti-mouse VEGF neutralization antibody (NAb) in addition to using EGM devoid of human VEGF. Tube formation of 005 cells cultured in DFS with DFO medium or in EGM with or without DFO was not inhibited at all despite the addition of 1 μg/mL NAb (Fig. 6*B*), which completely inhibited activity of 100 ng/mL VEGF on growth of human umbilical vein endothelial cells (HUVECs), whereas 10 ng/mL VEGF can enhance tube formation of HUVECs (Fig. S2). We also added the anti-VEGF receptor–specific small molecule inhibitor AG28262 (Pfizer), which inhibits autophosphorylation of VEGF-R1, VEGF-R2, and VEGF-R3 selectively at a subnanomolar concentration (20). There was no inhibition of tube formation even at a 20-nM concentration of the inhibitor (Fig. 6*C*). Because the TDECs were expressing FGFR-1 in our mouse GBMs (Fig. 2*D*), we used a high concentration of the AG28262 (200 and 1,000 nM), which inhibits not only VEGF receptors but FGFR-1. However, there was no significant inhibition of tube formation (Fig. 6*C*). These results reaffirm that GBM-initiating cells are able to differentiate into ECs by a VEGF- or FGF-independent mechanism.

Resistance of TDECs to Anti-VEGF Receptor Inhibitor. To confirm the resistance of TDECs to anti-VEGF therapies and that this resistance is playing an important role in the resistance of patients

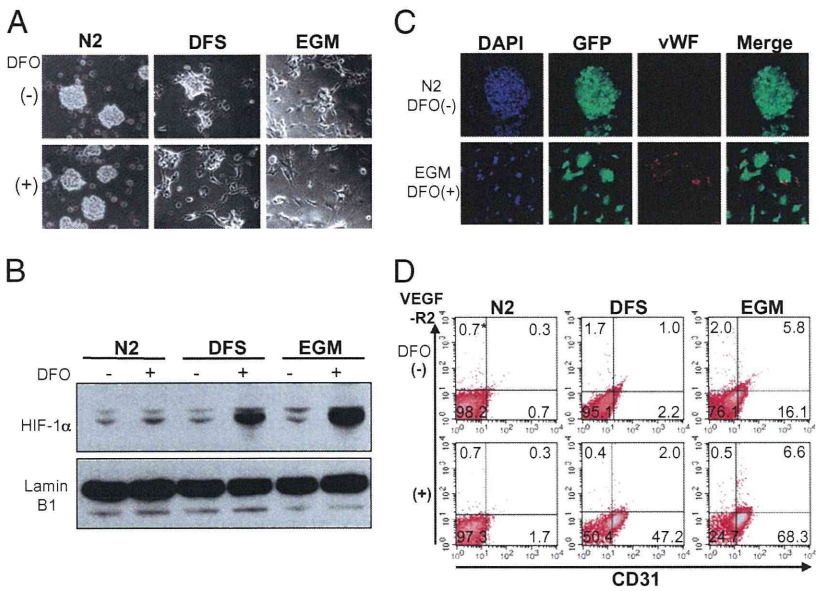

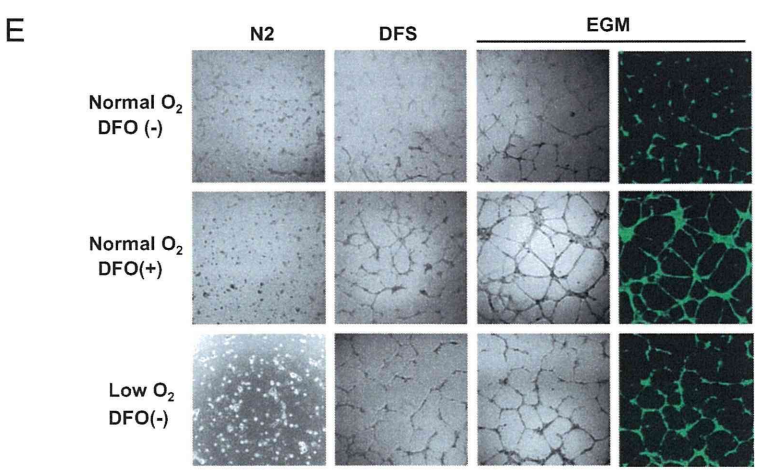

Fig. 5. Endothelial differentiation of tumor-initiating cells in vitro. (*A*) Morphological changes of 005 cells cultured in N2 medium, DFS medium, and EGM with or without DFO. (*B*) Expression of HIF-1α in 005 cells cultured in the indicated conditions. Nuclear protein was extracted from the cells and analyzed by Western blotting using anti-HIF-1α antibody (*Upper*) or anti-lamin B1 antibody (*Lower*). (*C*) Representative confocal microscopy images of 005 cells cultured in N2 medium without DFO (*Upper*) or in EGM with DFO (*Lower*). The confocal microscopy images are maximum projection images of consecutive single-slice images at an Airy factor of 1.0. (Magnification: 40×.) (*D*) Flow cytometry of CD31 and VEGF-R2 expression in 005 cells cultured in various conditions. (*E*) Tube formation assay of 005 cells cultured in the indicated conditions and seeded on Matrigel. The 005 cells were cultured in DFS medium with DFO and in EGM with or without DFO under normoxia-formed tube structure, and all these cells were GFP^+. The hypoxic condition (low O_2) in DFS medium and EGM without DFO also induced tube formation.

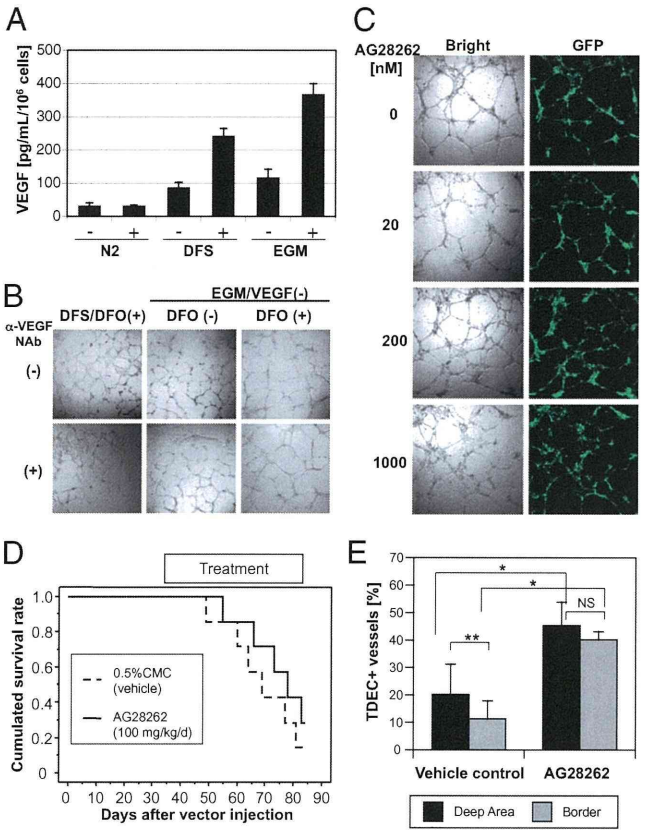

Fig. 6. Effect of inhibition of VEGF on TDEC formation. (*A*) Concentration of mVEGF in culture supernatant of 005 cells in various conditions. VEGF was released from 005 cells constitutively, and DFO treatment enhanced the production of VEGF significantly in DFS medium and EGM. Data represent mean ± SD of triplicate assays. (*B*) Effect of anti-VEGF NAb on tube formation. The 005 cells cultured in the indicated conditions were seeded on Matrigel, and tube formation was observed after 20 h. We omitted human VEGF from the EGM in this assay and used 1 μg/mL anti-VEGF NAb. (*C*) Effect of anti-VEGF receptor small molecule inhibitor AG28262 on tube formation of 005 cells. We cultured cells and observed tube formation under the same condition indicated in *B*, except for the addition of NAb. (*D*) Survival curve of the GBM mice treated with AG28262. GFAP-Cre transgenic mice received stereotaxic injection of LVs in the hippocampus of the brain. Mice were administrated 100 $mg \cdot kg^{-1} \cdot d^{-1}$ AG28262 orally for 6 wk from the sixth week after lentiviral injection. Control mice were administrated vehicle (0.5% carboxyl methyl cellulose). The survival curve was obtained by the Kaplan–Meier method, and the statistical difference was examined by the log-rank test. (*E*) Frequency of TDEC-forming vessels in the mouse GBM. Tumors were obtained from the mice that developed tumors and examined by immunofluorescence assay using a confocal microscope. Data represent mean ± SD from six (control) or five (AG28262) mice. *<0.5% by the Mann–Whitney *U* test; **<0.5% by the Wilcoxon signed-rank test; NS, not significant by the Wilcoxon signed-rank test.

with GBM to anti-VEGF therapies, we have examined the effect of VEGF receptor inhibitor on tumor development and TDEC formation in vivo using our mouse GBM model. We have administrated the VEGF receptor inhibitor AG28262 from week 6–12 following LV transduction. As shown in Fig. 6*D*, there was no significant difference in survival between the control group and AG28262 group ($P = 0.3688$), indicating that the VEGF inhibitor had almost no effect on tumor growth as observed in clinical studies. Examination of tumor vessels revealed that TDECs increased in the treated mice compared with control mice, however. Although the regular ECs decreased in the treated mice, TDECs significantly increased in ratio compared with control mice (Fig. 6*E*). Furthermore, the increase of TDECs in the AG28262-treated mice was particularly significant in the border area of the tumor, which contains fewer TDECs than the deep area in control mice (Fig. 6*E*). These results indicate that TDEC formation is resistant to the anti-VEGF therapy and strongly suggest the contribution of TDECs in the clinical resistance of GBM to anti-VEGF therapies.

TDECs in Xenograft Tumors of Human GBM Spheres. We next asked if TDECs were also found in human GBMs. We obtained three lenti-GFP–transduced human GBM spheres (21) and transplanted them in the brains of NOD-SCID mice. The resulting tumors examined by immunofluorescence show that regular vascular ECs express vWF but not human nestin or GFP (Fig. 7*A*). In contrast, some ECs express not only vWF but human nestin and GFP (Fig. 7*B*). Fig. 7*C* further shows that regular GFP^- ECs were human CD31 (hCD31)-negative but mouse CD31 (mCD31)-positive, whereas GFP^+ EC cells expressed hCD31 but not mCD31 (Fig. 7*D*). It thus appears that like the mouse GBMs, human GBMs are also capable of forming TDECs. The average ratio of TDECs in total ECs in three transplanted GBMs was 15–44% in the deep area and 4–22% in the border area (Fig. S3). Therefore, as in the mouse model, hypoxia may also play an important role in TDEC formation in human GBMs.

Presence of EGF Receptor-Positive ECs in Clinical Samples of Patients with GBM. Finally, we wanted to determine if direct clinical samples from patients with GBM also contained TDECs. We took advantage of the genetic abnormalities in the form of EGF receptor (EGFR) amplification in these tumors and asked if some ECs contained both human vWF and EGFR. Fig. 7*E* shows the ECs in the normal human brain by immunofluorescence with vWF antigen (Fig. 7*E*, *i*, *iii*, and *iv*) but no reactivity to anti-EGFR antigen (Fig. 7*E*, *ii*, *iii*, and *iv*). In contrast, Fig. 7F shows that some ECs in the clinical tumor sample express both vWF and EGFR (Fig. 7*F i–iv*), offering strong evidence for the presence of TDECs in human GBMs.

Discussion

In tumor angiogenesis, BM-derived circulating endothelial precursors (CEPs) are known to be the main source of the vascular ECs (22). A recent study suggested that the BM-derived CEPs did not contribute to the vascular endothelium, however (23). To date, the presence of TDECs has been suggested in several neoplasias, such as CML, lymphoma, and myeloma, by analyzing clinical samples (8–10). In these tumors, tumor-specific fusion genes resulting from chromosomal translocation were used for the tumor-specific markers. Here, we have demonstrated the presence of blood vessel ECs expressing the tumor marker GFP in our recently developed mouse GBM model, in human GBM xenografts, and clinical samples from patients. In contrast to the conventional theory of tumor angiogenesis in which the ECs are derived from mesodermal BM progenitor cells (22), the presence of TDECs in GBM suggests that the ECs transdifferentiated from the neuroectoderm and that tumor cells can also be involved in tumor angiogenesis. The endothelial transdifferentiation of the tumor cells may result from the aberrant stem cell character of the tumor progenitor cells. The other possible mechanism is that the endothelial differentiation of GBM cells is not the result of transdifferentiation but reflects the normal differentiation pathway of the NSC, which has previously been described to differentiate into ECs (16). If this is also observed in the normal differentiation of human NSCs, perhaps the terminology of transdifferentiation needs reconsideration.

Vasculogenic mimicry (VM) has been reported in melanoma as fluid-conducting channels formed by the tumor cell itself. In contrast to the regular blood vessels, VM lacks ECs; therefore, VM was easily distinguishable from regular blood vessels. VM was also reported in nonmelanoma tumors, including GBM (24–26). The TDECs in this study are likely to be different from the VM because the TDECs are indistinguishable from regular ECs, except for the tumor-specific markers (e.g., GFP) or chromo-

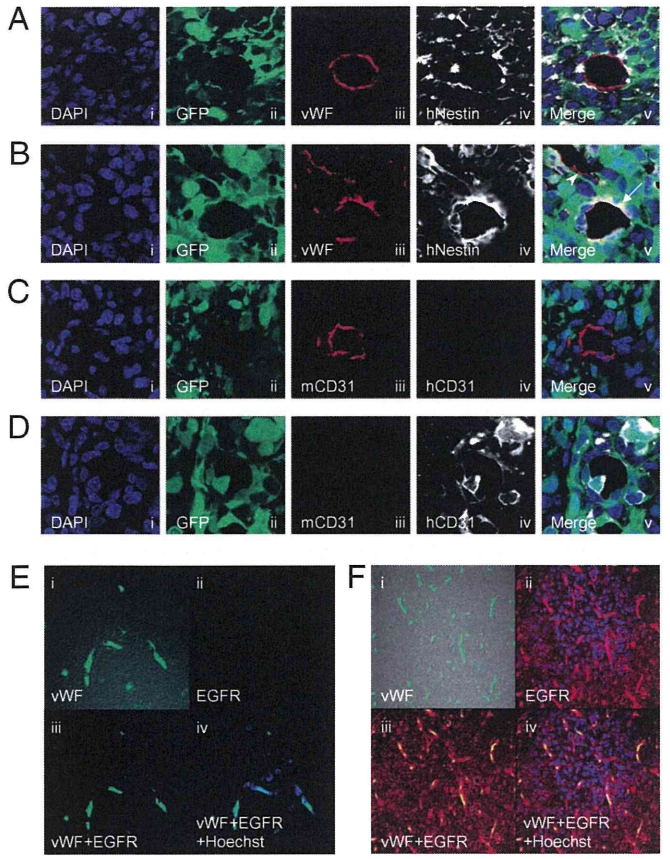

Fig. 7. TDEC formation in a xenograft model using human GBM spheres and patient samples. Representative images of regular ECs (*A* and *C*) and TDECs (*B* and *D*) in brain tumors developed in NOD-SCID mice transplanted with human GBM spheres. (*A–D*) (*i*) DAPI nuclear staining; (*ii*) GFP; (*iii*) and (*iv*) expression of indicated antigens; (*v*) merging image. (*A* and *B*) Tumors were stained with anti-vWF antibody, which reacts with both mouse and human vWF, and with an antibody specific for human nestin. (*A*) Regular ECs expressed vWF (*iii*) but not GFP (*ii*) or human nestin (*iv*). (*B*) TDECs expressed vWF (*iii*), GFP (*ii*), and human Nestin (*iv*; *v*, showing the merge with an arrow). A regular EC is indicated by the arrowhead (*v*). (*C* and *D*) Tumors were also stained with antibodies specific for mouse CD31 or human CD31. (*C*) Regular ECs expressed mouse CD31 (*iii*) but not human CD31 (*iv*). (*D*) TDECs expressed human CD31 (*iv*) but not mouse CD31 (*iii*). (*E* and *F*) Representative images of blood vessels of clinical samples of patients with GBM. (*i*) vWF; (*ii*) EGFR; (*iii*) merging image; (*iv*) merging image with Hoechst 33258 nuclear staining. (*E*) Vessels of normal brain expressed vWF (*i*) but not EGFR (*ii*). (*F*) vWF^+ ECs (*i*) strongly expressed EGFR (*ii*), and surrounding tumor cells expressed EGFR (*ii*).

somal rearrangements. There is another aberrant tumor vessel, the "mosaic tumor vessel," which was reported in colon cancer (27). The mosaic blood vessels are lumens formed with both ECs and tumor cells lacking EC markers. Because the TDECs are expressing EC markers and behave as regular ECs, the TDECs are likely to be different from the mosaic vessels.

The transdifferentiation of tumor cells into vessel formation in GBM was not previously recognized, probably because of the lack of a good tumor marker. We also suggest that hypoxia is an important factor of endothelial differentiation in addition to regular tumor vessel formation. In the hypoxic condition, induction of VEGF expression through the stabilization of HIF-1α is an important factor for tumor angiogenesis (15). In contrast to regular endothelial differentiation, however, in vitro assays have suggested that the formation of TDECs is independent of VEGF and FGF (Fig. 6 *B* and *C*). In addition, administration of the anti-VEGF receptor inhibitor AG28262 did not improve survival of the GBM mice (Fig. 6*D*), and TDEC formation increased in contrast to regular ECs (Fig. 6*E*). Therefore, the involvement of TDECs in tumor angiogenesis might be one of the resistance mechanisms against anti-VEGF therapies and may require novel combination therapies.

While this paper was under review, two articles (28, 29) were published that further support the notion that a proportion of ECs contributing to the formation of blood vessels in human GBMs originate from tumor cells. The findings of these two groups show that ECs (ranging from 20–90%) in the tumors carry genetic abnormalities found in the tumor cells themselves. Thus, together with the findings reported here, it is clear that part of the vasculature in GBMs originates from tumor cells, bypassing the normal mechanisms of angiogenesis, thus offering an additional therapeutic opportunity to treat the disease.

Materials and Methods

Establishment of Mouse GBM Model by Lentiviral Vector Injection. The mouse GBM model was established as described (13). Briefly, we injected the Cre-inducible LVs Tomo H-RasV12 LV and Tomo AKT LV stereotaxically into the hippocampus of GFAP-Cre/$p53^{+/-}$ transgenic mice. More recently, mouse GBM models have also been generated in GFAP-Cre mice using a single lentiviral vector containing activated H-Ras and sip53. We have killed mice to take tumor samples when the mice show tumor-related signs, such as a domed head, a hunched position, lethargy, and weight loss. In most cases, it takes 3–4 mo after vector injection before tumor-related signs appear.

Cell Culture. Mouse GBM-initiating cell lines 005 and 006 were established as described (13). The 005 and 006 cells were maintained in N2 medium, which contains DMEM/F-12 (Omega Scientific), 1% N2 supplement (Invitrogen), 20 ng/mL human FGF-2 (Peprotech), 20 ng/mL human EGF (Promega), and 40 μg/mL heparin (Sigma). In the differentiation-induction assay, cells were cultured in DFS medium [10% (vol/vol) FBS] or EGM-2 (Lonza). To reproduce the hypoxic condition, we added 100 μg/mL DFO mesylate (Sigma) into the above media. The 005 cells were also cultured in the 2% O_2 condition using an N_2O_2 incubator. Mouse GBM-initiating 005 cells were transplanted into the hippocampus of NOD-SCID mice or DsRed transgenic mice. HUVECs were cultured in the EGM-2.

Transplantation of Mouse GBM-Initiating Cells. Mouse GBM-initiating 005 and 006 cells were transplanted into brains of NOD-SCID mice or DsRed transgenic mice. A total of 3×10^5 cells were suspended in 1–1.5 μL of PBS and injected stereotaxically in the right hippocampus. These mice developed GBM about 1–2 mo after transplantation. In some cases, as few as 5,000 cells were injected, except the tumors took longer to develop.

Immunofluorescence Assay. Mouse brain tumors were processed as described (13). The primary antibodies used in this study are as follows: rabbit anti-vWF (Abcam), rat anti-mCD31 (MEC13.3; Becton Dickinson), rat anti-mCD34 (RAM34; Becton Dickinson), rat anti-mCD144 (11D4.1; Becton Dickinson), chicken anti-nestin (Abcam), rabbit anti-DYKDDDK (Cell Signaling), goat anti-VEGF-R2 (Abcam), and rabbit anti-FGF-R1 (Abcam). The secondary antibodies used were as follows (all from Invitrogen): Alexa Fluor 568 anti-rabbit IgG, Alexa Fluor 568 anti-rat IgG, Alexa Fluor 647 anti-rabbit IgG, Alexa Fluor 647 anti-rat IgG, Alexa Fluor 647 anti-chicken IgG, and Alexa Fluor 647 anti-goat IgG. The nucleus was stained by DAPI. The images were obtained by confocal laser scanning microscopy (TCS SP2 ABS; Leica or LSM 5 PASCAL; Carl Zeiss), and the obtained images were processed by Photoshop software (Adobe).

Hypoxyprobe Assay. To detect hypoxic regions of the brain tumors, a Hypoxyprobe-1 Omni kit (Natural Pharmacia International) was used. We injected 45 mg of Hypoxyprobe-1 into the tail veins of tumor-harboring mice 30 min before euthanasia. Brain sections were stained with rabbit anti-Hypoxyprobe antibody, followed by staining with Alexa Fluor 647-labeled anti-rabbit IgG antibody (Invitrogen). The images were obtained by confocal laser scanning microscopy.

Blood Flow Detection Assay. We injected 50 μg of biotinylated lectin (Vector Laboratories) into the tail veins of tumor-harboring mice 15 min before euthanasia. Brain sections were stained with Alexa Fluor 647-labeled streptavidin (Invitrogen). The images were obtained by confocal laser scanning microscopy.

Flow Cytometry. The brain tumors were dissociated using a Neural Tissue Dissociation Kit (Miltenyi Biotec), and 005 cells were collected after differ-

entiation induction. These cells were stained with the following fluorescence-labeled antibodies: peridinin chlorophyll protein-Cy5.5 anti-mCD45 (30-F11; Becton Dickinson), phycoerythrin (PE) anti-mCD34 (RAM34; Becton Dickinson), Alexa Fluor 647 anti-mCD31 (MEC13.3; BioLegend), and PE anti-mH-2K^d (SF1-1.1; Becton Dickinson). They were then analyzed on a BD LSR I flow cytometer (Becton Dickinson).

Western Blotting. Nuclear proteins from 005 cells cultured in various conditions were extracted and subjected to SDS/PAGE. Proteins were transferred to a PVDF membrane and probed with mouse anti-HIF-1α antibody (Novus), followed by probing with HRP-labeled anti-mouse IgG (Santa Cruz). The blot was reprobed with rabbit anti-lamin B1 antibody (Abcam) and HRP-labeled anti-rabbit IgG (GE Healthcare) after treatment with a ReBlot Plus kit (Millipore). A fluorescence signal was generated using an ECL kit (GE Healthcare).

ELISA. The VEGF concentration of culture supernatant of 005 cells was measured by ELISA using a Duo Set Mouse VEGF kit (R&D Systems). Optical density at 450 nm was measured by an HTS 7000+ microplate reader (Perkin–Elmer).

Tube Formation Assay. The 005 cells cultured in various conditions were seeded on Matrigel (Becton Dickinson). HUVECs were suspended in RPMI 1640 medium supplemented with 1% FBS and seeded on Matrigel in the presence or absence of 10 ng/mL mouse VEGF (mVEGF) and 1 μg/mL anti-mVEGF NAb. After 20 h, images of the cells were taken using an inverted fluorescence microscope (Axiovert 100; Zeiss).

Human GBM Sphere Cultures. The human GBM sphere lines (BT37, BT70, and BT74) were derived from GBM biopsies, implanted into NOD-SCID mice, and passaged serially in mice to maintain authentic biology (30). Dissected xenografts were washed in artificial cerebrospinal fluid and manually dissociated into single cells. Red blood cells were removed using Lympholyte-M (Cedarlane). The cells were cultured in DMEM/F12 (with L-glutamine; Invitrogen) medium containing glucose (0.3%), penicillin/streptomycin (50 μg/mL), Apo-transferrin (0.1 mg/mL), progesterone (20 nM), sodium selenite (30 nM), putrescine (60 μM), insulin (25 μM/mL), sodium bicarbonate (3 mM), Hepes (10 mM), 20 ng/mL EGF, 10 ng/mL leukemia inhibitory factor (LIF), and 20 ng/mL FGF. Live cells were counted using a hemocytometer and trypan blue exclusion.

Lentiviral Transduction. Lentiviral vector stocks of pLKO-GFP lentiviral vectors were produced as previously described (31). For neurosphere transduction, 110 mL of virus was concentrated by ultracentrifugation using an SW-28 rotor (Beckman Coulter) and rotated at 19,500 rpm at 4 °C for 3 h. The pellet was resuspended in 360 μL of serum-free DMEM overnight. Fifty microliters of virus was used to infect 100,000 viable cells.

In Vivo Human Xenograft Model. Animal husbandry was performed according to University of California at San Diego guidelines under Institutional Animal Care and Use Committee-approved protocols. For orthotopic transplants, 2×10^5 cells in 2 μL of HBSS were injected stereotaxically. Mice were killed when morbid, and brain tumors were perfused with PBS and 4% paraformaldehyde (wt/vol), excised, and processed for histological studies.

Human GBM Clinical Samples. We retrospectively reviewed the cases of patients with GBM who were treated at Okayama University Hospital. All tumor samples were fixed with formalin and embedded in paraffin. These samples were approved by the patients for research use. The primary antibodies used in this assay were anti-EGFR antibody (MS-378-P; NeoMarker) and anti-human vWF (A0082; Dako). The secondary antibodies were anti-mouse IgG Cy3 (c-2181; Sigma) and anti-rabbit IgG FITC (F-4890; Sigma). The nucleus was stained by Hoechst 33258. The images were obtained by confocal laser scanning microscopy (LSM510; Zeiss).

ACKNOWLEDGMENTS. We thank Drs. D. Cheresh, F. H. Gage, K. Shimozaki, and H. Kato for useful discussions and Dr. K. Suzuki, G. Estepa, M. Schmitt, B. Coyne, and the other members of the Verma and Gage laboratories of the Salk Institute for help. We also thank Pfizer for AG28262. T.M. was supported by the American Brain Tumor Association. I.M.V. is an American Cancer Society Professor of Molecular Biology and holds the Irwin Mark Jacobs Chair in Exemplary Life Sciences. I.M.V. was supported by the National Institutes of Health (Grant HL053670), National Cancer Institute (Grant P30CA014195), Merieux Foundation, Ellison Medical Foundation, Ipsen/Biomeasure, Sanofi Aventis, and H. N. and Frances C. Berger Foundation. S.K. was supported by the National Institutes of Health (Grants K08CA124804 and 3P30CA023100-25S8) and James S. McDonnell Foundation. M.Y. was supported by the National Cancer Institute (Grant R01CA132971-01A1).

1. Wen PY, Kesari S (2008) Malignant gliomas in adults. *N Engl J Med* 359:492–507.
2. Jain RK, et al. (2007) Angiogenesis in brain tumours. *Nat Rev Neurosci* 8:610–622.
3. Vredenburgh JJ, et al. (2007) Phase II trial of bevacizumab and irinotecan in recurrent malignant glioma. *Clin Cancer Res* 13:1253–1259.
4. Bergers G, Hanahan D (2008) Modes of resistance to anti-angiogenic therapy. *Nat Rev Cancer* 8:592–603.
5. Shojaei F, Ferrara N (2008) Refractoriness to antivascular endothelial growth factor treatment: Role of myeloid cells. *Cancer Res* 68:5501–5504.
6. Pope WB, Lai A, Nghiemphu P, Mischel P, Cloughesy TF (2006) MRI in patients with high-grade gliomas treated with bevacizumab and chemotherapy. *Neurology* 66:1258–1260.
7. Pàez-Ribes M, et al. (2009) Antiangiogenic therapy elicits malignant progression of tumors to increased local invasion and distant metastasis. *Cancer Cell* 15:220–231.
8. Gunsilius E, et al. (2000) Evidence from a leukaemia model for maintenance of vascular endothelium by bone-marrow-derived endothelial cells. *Lancet* 355:1688–1691.
9. Streubel B, et al. (2004) Lymphoma-specific genetic aberrations in microvascular endothelial cells in B-cell lymphomas. *N Engl J Med* 351:250–259.
10. Rigolin GM, et al. (2006) Neoplastic circulating endothelial cells in multiple myeloma with 13q14 deletion. *Blood* 107:2531–2535.
11. Pezzolo A, et al. (2007) Tumor origin of endothelial cells in human neuroblastoma. *J Clin Oncol* 25:376–383.
12. Bussolati B, Grange C, Sapino A, Camussi G (2009) Endothelial cell differentiation of human breast tumour stem/progenitor cells. *J Cell Mol Med* 13:309–319.
13. Marumoto T, et al. (2009) Development of a novel mouse glioma model using lentiviral vectors. *Nat Med* 15:110–116.
14. Dahlstrand J, Collins VP, Lendahl U (1992) Expression of the class VI intermediate filament nestin in human central nervous system tumors. *Cancer Res* 52:5334–5341.
15. Bergers G, Benjamin LE (2003) Tumorigenesis and the angiogenic switch. *Nat Rev Cancer* 3:401–410.
16. Wurmser AE, et al. (2004) Cell fusion-independent differentiation of neural stem cells to the endothelial lineage. *Nature* 430:350–356.
17. Yang M, Reynoso J, Bouvet M, Hoffman RM (2009) A transgenic red fluorescent protein-expressing nude mouse for color-coded imaging of the tumor microenvironment. *J Cell Biochem* 106:279–284.
18. Ivan M, et al. (2001) HIFalpha targeted for VHL-mediated destruction by proline hydroxylation: Implications for O2 sensing. *Science* 292:464–468.
19. Jaakkola P, et al. (2001) Targeting of HIF-alpha to the von Hippel-Lindau ubiquitylation complex by O2-regulated prolyl hydroxylation. *Science* 292:468–472.
20. Zou HY, et al. (2004) AG-028262, a novel selective VEGFR tyrosine kinase antagonist that potently inhibits KDR signaling and angiogenesis in vitro and in vivo. *Proc Am Assoc Cancer Res* 45:A2578.
21. Chen J, et al. (2010) Inhibition of Notch Signaling Blocks Growth of Glioblastoma Cell Lines and Tumor Neurospheres. *Genes Cancer* 1:822–835.
22. Bertolini F, Shaked Y, Mancuso P, Kerbel RS (2006) The multifaceted circulating endothelial cell in cancer: Towards marker and target identification. *Nat Rev Cancer* 6:835–845.
23. Purhonen S, et al. (2008) Bone marrow-derived circulating endothelial precursors do not contribute to vascular endothelium and are not needed for tumor growth. *Proc Natl Acad Sci USA* 105:6620–6625.
24. Hendrix MJ, Seftor EA, Hess AR, Seftor RE (2003) Vasculogenic mimicry and tumour-cell plasticity: Lessons from melanoma. *Nat Rev Cancer* 3:411–421.
25. Yue WY, Chen ZP (2005) Does vasculogenic mimicry exist in astrocytoma? *J Histochem Cytochem* 53:997–1002.
26. El Hallani S, et al. (2010) A new alternative mechanism in glioblastoma vascularization: Tubular vasculogenic mimicry. *Brain* 133:973–982.
27. Chang YS, et al. (2000) Mosaic blood vessels in tumors: Frequency of cancer cells in contact with flowing blood. *Proc Natl Acad Sci USA* 97:14608–14613.
28. Ricci-Vitiani L, et al. (2010) Tumour vascularization via endothelial differentiation of glioblastoma stem-like cells. *Nature* 468:824–828.
29. Wang R, et al. (2010) Glioblastoma stem-like cells give rise to tumour endothelium. *Nature* 468:829–833.
30. Lee J, et al. (2006) Tumor stem cells derived from glioblastomas cultured in bFGF and EGF more closely mirror the phenotype and genotype of primary tumors than do serum-cultured cell lines. *Cancer Cell* 9:391–403.
31. Moffat J, et al. (2006) A lentiviral RNAi library for human and mouse genes applied to an arrayed viral high-content screen. *Cell* 124:1283–1298.

J Neurooncol (2011) 103:175–185
DOI 10.1007/s11060-010-0376-5

LABORATORY INVESTIGATION - HUMAN/ANIMAL TISSUE

Convection enhanced delivery of carboranylporphyrins for neutron capture therapy of brain tumors

Shinji Kawabata · Weilian Yang · Rolf F. Barth · Gong Wu · Tianyao Huo · Peter J. Binns · Kent J. Riley · Owendi Ongayi · Vijay Gottumukkala · M. Graça H. Vicente

Received: 1 February 2010 / Accepted: 19 August 2010 / Published online: 17 September 2010
© Springer Science+Business Media, LLC. 2010

Abstract Boron neutron capture therapy (BNCT) is based on the nuclear capture and fission reactions that occur when non-radioactive ^{10}B is irradiated with low energy thermal neutrons to produce α-particles ($^{10}B[n,\alpha]^{7}Li$). Carboranylporphyrins are a class of substituted porphyrins containing multiple carborane clusters. Three of these compounds, designated H_2TBP, H_2TCP, and H_2DCP, have been evaluated in the present study. The goals were two-fold. *First*, to determine their biodistribution following intracerebral (i.c.) administration by short term (30 min) convection enhanced delivery (CED) or sustained delivery over 24 h by Alzet^{TM} osmotic pumps to F98 glioma bearing rats. *Second*, to determine the efficacy of H_2TCP and H_2TBP as boron delivery agents for BNCT in F98 glioma bearing rats. Tumor boron concentrations immediately after i.c. pump delivery were high and they remained so at 24 h. The corresponding normal brain concentrations were low and the blood and liver concentrations were undetectable. Based on these data, therapy studies were initiated at the Massachusetts Institute of Technology (MIT) Research Reactor (MITR) with H_2TCP and H_2TBP 24 h after CED or pump delivery. Mean survival times (MST) ± standard deviations of animals that had received H_2TCP or H_2TBP, followed by BNCT, were of 35 ± 4 and 44 ± 10 days, compared to 23 ± 3 and 27 ± 3 days, respectively, for untreated and irradiated controls. However, since the tumor boron concentrations of the carboranylporphyrins were 3–5× higher than intravenous (i.v.) boronophenylalanine (BPA), we had expected that the MSTs would have been greater. Histopathologic examination of brains of BNCT treated rats revealed that there were large numbers of porphyrin-laden macrophages, as well as extracellular accumulations of porphyrins, indicating that the seemingly high tumor boron concentrations did not represent the true tumor cellular uptake. Nevertheless, our data are the first to show that carboranyl porphyrins can be used as delivery agents for BNCT of an experimental brain tumor. Based on these results, we now are in the process of synthesizing and evaluating carboranylporphyrins that could have enhanced cellular uptake and improved therapeutic efficacy.

Keywords Convection enhanced delivery · Carboranylporphyrins · Boron neutron capture therapy · F98 rat glioma

W. Yang · R. F. Barth (✉) · G. Wu · T. Huo
Department of Pathology, The Ohio State University, 165 Hamilton Hall 1645 Neil Avenue, Columbus, OH 43210, USA
e-mail: rolf.barth@osumc.edu

P. J. Binns · K. J. Riley
Nuclear Reactor Laboratory, Massachusetts Institute of Technology, Cambridge, MA 02139, USA

O. Ongayi · V. Gottumukkala · M. G. H. Vicente
Department of Chemistry, Louisiana State University, Baton Rouge, LA 70803, USA

S. Kawabata
Department of Neurosurgery, Osaka Medical College, Takatsuki City, Osaka, Japan

Present Address:
P. J. Binns
Department of Radiation Oncology, Mount Auburn Hospital, Cambridge, MA 02138, USA

K. J. Riley
Radiation Monitoring Devices, Inc, Watertown, MA 02472, USA

Introduction

Boron neutron capture therapy is based on the nuclear capture and fission reactions that occur when non-radioactive boron-10 is irradiated with neutrons of the appropriate energy to yield high energy alpha particles (^{4}He) and recoiling lithium-7 (^{7}Li) nuclei. Since these particles have pathlengths of approximately one cell diameter, their lethality primarily is limited to boron containing cells. BNCT, therefore, can be regarded as both a biologically and a physically targeted type of radiation therapy. Its success is dependent upon the selective delivery of sufficient amounts of ^{10}B to cancer cells with only small amounts localized in the surrounding normal tissues. A wide variety of boron delivery agents have been synthesized [1], but only two of these currently are being used in clinically. The first, which has been used primarily in Japan, is sodium borocaptate or BSH, and the second is a dihydroxyboryl derivative of phenylalanine referred to as boronophenylalanine or BPA [2]. The latter has been used in clinical trials in Japan, Europe and the United States, primarily for the treatment of high grade gliomas, and more recently for recurrent tumors of the head and neck region. Following i.v. administration of either BPA or BSH by i.v. infusion, the tumor site is irradiated with neutrons, the source of which is a nuclear reactor.

Several recent clinical studies on the treatment of patients with glioblastomas (GBM) by means of BNCT have reported encouraging results [3–6]. Careful analysis of survival data from a study, carried out in Sweden [3] in which BPA was administered at a higher dose over a longer period of time [4], suggested that a subset of patients had survival times that were at least as good as those obtained with conventional therapy consisting of X-irradiation in combination with temozolomide (TMZ) [7]. Similarly, BNCT studies carried out by Miyatake and Kawabata and their co-workers [5, 6], in which BPA and BSH were administered in combination, followed by an X-ray boost [6] showed favorable responses in patients with newly diagnosed GBM and especially those in high risk groups [6]. However, a randomized Phase III clinical trial ultimately will be necessary to unequivocally establish that BNCT can produce equivalent or superior survival data compared to the current standard treatment of surgery followed by RT and TMZ. Interested readers are referred to the recently published proceedings of the Thirteenth International Congress on Neutron Capture Therapy for more detailed information relating to BNCT [8].

There has been a long-standing interest on the part of a number of research groups on the design, synthesis and biological evaluation of boron-containing porphyrins as delivery agents for BNCT [9–28]. Detailed information on this subject is provided in two comprehensive reviews on boronated porphyrins [21, 22]. The carboranylporphyrins used in the present study belong to a class of *meso*-substituted porphyrins containing four *nido*-carborane clusters and 36 boron atoms per molecule (37–31% boron by weight), linked to the porphyrin macrocycle *via* hydrolytically-stable carbon–carbon bonds. These compounds have been designated 5,10,15,20-tetra-(4-*nido*-carboranylphenyl)tetrabenzoporphyrin (H_2TBP), 5,10,15,20-tetra-(4-*nido*-carboranylphenyl)porphyrin (H_2TCP) and 5,15-di-[3,5-(*nido*-carboranylmethyl)phenyl]porphyrin (H_2DCP) and their structures are shown in Fig. 1. The synthesis and preliminary biological evaluation of H_2TCP [23–26], H_2DCP [26, 27] and H_2TBP [28, 29], previously have been reported. Earlier studies [23–25, 27–29] suggested that H_2TCP, H_2DCP and H_2TBP were promising boron delivery agents due to their low toxicity and enhanced tumor uptake.

Based on the reports of Ozawa et al. [30, 31] and our own experience with CED [32], we decided to focus on direct i.c. delivery of the carboranylporphyrins rather than

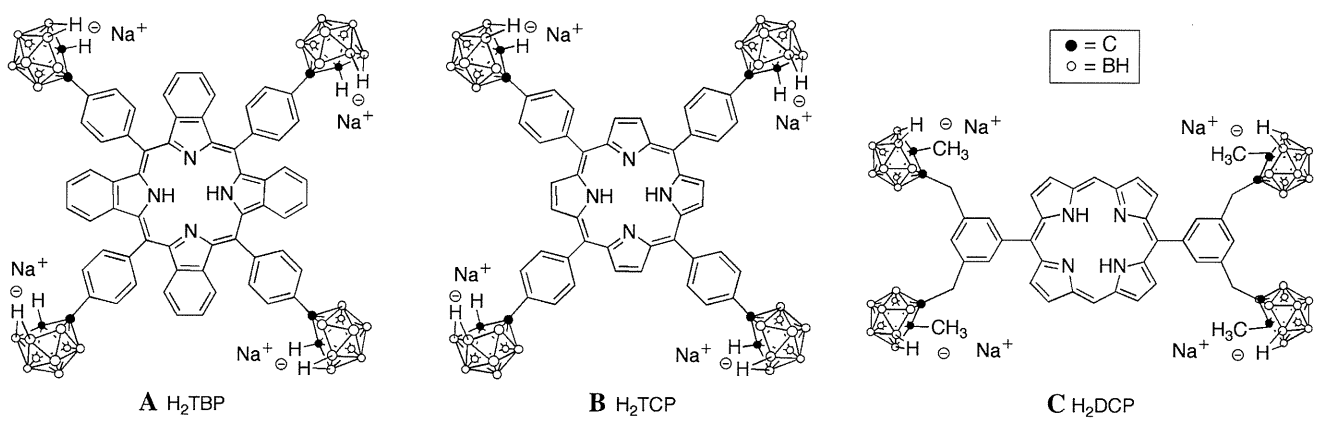

Fig. 1 Chemical structures of the carboranylporphyrins used in this study: **A** tetra(4-*nido*-carboranylphenyl)tetra-benzo-porphyrin, H_2TBP; **B** tetra(4-*nido*-carboranylphenyl) porphyrin (H_2TCP); and **C** di[3,5-(*nido*-carboranylmethyl)phenyl]porphyrin (H_2DCP)

systemic administration. CED is an innovative method for local drug delivery to brain tumors by which a pressure gradient, or bulk flow, is used to drive an infusate through the extracellular compartment [33]. It allows delivery of the infusate to the tumor and surrounding brain at much higher concentrations than could be achieved by systemic administration. As demonstrated in both animal studies [32, 34] and clinical trials [35, 36], CED not only increased the delivery of both low and high molecular weight agents, but also improved their therapeutic efficacy. Initially, we carried out some preliminary studies with several carboranylporphyrins using the F98 rat glioma model [37]. We now present a more detailed evaluation of the biodistribution and efficacy of H_2TCP, H_2DCP and H_2TBP as potential boron delivery agents for neutron capture therapy (NCT).

Materials and methods

Synthesis of carboranylporphyrins

All *nido*-carboranylporphyrins were synthesized from the corresponding *closo*-carboranylporphyrins via base-induced degradation for H_2TCP and H_2DCP or fluoride-induced degradation for H_2TBP [38]. Therefore, all of them were stereoisomers, as shown by ^{1}H-NMR spectra and ab initio calculations, which might contribute to their therapeutic efficacy. The percent boron by weight was 27% for H_2TBP and 31% for H_2TCP and H_2DCP. Two of these were converted to their zinc complexes, ZnDCP and ZnTCP, for the biodistribution studies described below. These were all stable for months at physiologic temperatures, but they were light sensitive and, therefore, they were shielded from light prior to their administration.

Biodistribution of ZnDCP and ZnTCP in glioma bearing mice

Biodistribution studies were carried out in female C57Bl/6 mice (Animal Production Branch, National Cancer Institute, Frederick, MD), weighing 20–25 g, bearing the syngeneic murine GL261 glioma. This tumor was induced by the i.c. implantation of methylcholanthrene pellets into the brain of a C57Bl/6 mouse [39]. It is composed of poorly differentiated cells histopathologically consistent with a glioblastoma. Tumor cells were implanted subcutaneously (s.c.) into the right dorsum with an inoculum of 1.8×10^6 cells. Biodistribution studies were carried out 15 days after implantation at which time the tumor volumes were ~ 80 mm^3. The zinc(II) complexes of H_2DCP and H_2TCP, ZnDCP and ZnTCP, respectively, were injected intraperitoneally (i.p.) over 8 h in three doses totaling 30 mg boron/kg body weight (b.w.). Since these compounds are photosensitizers, the animals were shielded from light during the course of the experiment. In order to compare their biodistribution with that of BPA, another group of mice received a single i.p. injection of BPA at a concentration of 500 mg/kg b.w. Mice were euthanized at 24 and 48 h following the first injection and tissue and blood samples were taken for boron determinations by means of direct current plasma-atomic emission spectroscopy (DCP-AES), as previously described by us [40]. All animal studies were done in accordance with the *Guide for the Care and Use of Laboratory Animals* (National Academy Press, Washington, DC, 1996) and the protocol was approved by the Institutional Laboratory Animal Care and Use Committee of The Ohio State University.

F98 rat glioma model

The F98 rat glioma (#CRL-2397, American Type Culture Collection, Manasus, VA) was derived from an undifferentiated neoplasm transplacentally induced in the progeny of a pregnant CD Fischer rat by the i.v. administration of *N*-ethyl-*N*-nitrosourea [41]. It has been propagated in vitro and in vivo since 1971 and, as described in a recent review [42], the F98 glioma has been used in a wide variety of studies in experimental neuro-oncology. This tumor has an infiltrative pattern of growth within the brain, and an i.c. inoculum of as few as ten cells can be fatal. In the present study, F98 cells were grown in Dulbecco's modified Eagle's medium (DMEM) (Gibco, Grand Island, NY) supplemented with 10% fetal bovine serum (FBS) (Hyclone, Logan, UT), 100 units/ml penicillin, 100 μg/ml streptomycin and 2 mM L-glutamine. Fischer rats (Animal Production Branch, National Cancer Institute, Frederick, MD), weighing 220–240 g, were used in these studies. A stereotactic implantation procedure, which has been described in detail elsewhere, was employed [43]. Briefly, rats were sedated by i.p. administration of a 1.2:1 mixture of ketamine/xylazine at a dose of 120 mg of ketamine/20 mg xylazine/kg b.w. Following this, a small burr hole was drilled into the calvarium and a plastic screw with an entry port (Arrow Machine Manufacturing, Inc., Richmond, VA) was embedded into the skull. F98 cells at a concentration of either 10^3 for therapy studies or 10^5 cells for biodistribution studies were injected stereotactically into the right caudate nucleus over 10–15 s through a small entry port of the plastic screw. Following this, the entry port was filled with bone wax immediately after withdrawal of the needle, and the operative field was flushed with betadine before the scalp incision was closed with a single sterilized clip. Eleven to thirteen days after tumor implantation of 10^5 cells, when clinical signs of a progressively growing i.c. tumor were evident, biodistribution studies were initiated.

Biodistribution studies in F98 glioma bearing rats following convection-enhanced delivery (CED) of carboranylporphyrins

Since the zinc(II) complexes of carboranylporphyrins had lower cellular uptake than the free base porphyrins, studies subsequently were carried out with H_2DCP and H_2TCP. In order to increase tumor uptake and decrease uptake by extracranial organs and tissues, these were administered i.c. by means of CED or Alzet^{TM} pump infusion to F98 glioma bearing rats. Eleven to thirteen days after tumor implantation, when signs of a progressively growing i.c. tumor were evident (weight loss, lethargy, hunching, and ataxia), biodistribution studies were initiated. In contrast to the biodistribution studies carried out in mice, which had received the test porphyrins by i.p. injection, it was not necessary to shield these rats from light. For short term CED of the carboranylporphyrins, a 28 gauge needle was inserted into the entry port of the plastic screw and then advanced 5 mm below the dura into the tumor. The boronated porphyrins were diluted with phosphate buffered saline (PBS), pH 7.4, to yield a concentration of 0.1–0.2 mg of compound in 10 μl. They compounds were administered by CED at a flow rate of 0.33 μl/min for 30 min using a syringe pump (Harvard Apparatus Co, Cambridge, MA). Biodistribution was determined immediately after and 24 and 48 h after termination of CED. Animals were euthanized by an overdose of halothane, following which tumors and normal tissues, consisting of brain, blood, liver, kidney and muscle, were removed and weighed. Uptake of boron was quantified by means of DCP-AES [40].

Biodistribution of carboranylporphyrins following i.c. infusion by osmotic pumps

Alzet osmotic pumps (model #2001 D) and brain infusion kits (rigid stainless-steel cannula, 7 mm, 28 gauge) were assembled and filled with 200 μl of the test carboranylporphyrins. The pumps were stored in the dark in a sterile solution of 0.9% saline at 37°C for 24 h prior to their use. Fourteen days after tumor implantation, the rats were anesthetized again and the scalp was reopened. The pumps were implanted s.c. between the scapulae. The infusion cannula and needle were inserted stereotactically into the entry port of the plastic screw and the needle was advanced 5 mm below the dura into the tumors of glioma bearing rats. H_2DCP, H_2TCP or H_2TBP at varying doses, ranging from 0.2 to 1.0 mg, were delivered in volume of 200 μl at a constant flow rate of 8 μl/h over 24 h following which the animals were euthanized immediately (t = 0) or 24 or 48 h later. Boron concentrations were determined in samples of tumor, brain, blood, liver, spleen, kidneys, lungs and heart by means of DCP-AES.

Therapy experiments

BNCT was performed 14 days following stereotactic implantation of 10^3 F98 glioma cells. Rats were transported to the Nuclear Reactor Laboratory at the Massachusetts Institute of Technology (MIT). Based on the results of the biodistribution study, a total of either 0.2 mg of the compound was administered by CED for 30 min or 0.5 mg of the compound was infused for 24 h by Alzet pumps. The animals were then randomized on the basis of weight into experimental groups of 9–10 animals each as follows: Group 1, H_2TCP, administered by Alzet pumps and BNCT; Group 2, H_2TBP by Alzet pumps and BNCT; Group 3, H_2TBC by CED and BNCT; Group 4, H_2TBP by CED + i.v. BPA and BNCT; Group 5, i.v. BPA, followed 2.5 h later by BNCT; Group 6, CED of saline and neutron irradiation; Group 7, unirradiated controls that received H_2TCP by CED. BNCT was initiated 24 h after termination of CED or infusion and 2.5 h after i.v. administration of ^{10}B enriched BPA at a dose of 500 mg/kg b.w. (Ryscor Science, Inc., Raleigh, NC). All irradiated rats were anesthetized with a mixture of ketamine and xylazine. BNCT was carried out at the MITR-II nuclear reactor in the M011 irradiation facility. This produces a beam of thermal neutrons of high purity and intensity with no measurable fast neutron component. Two rats at a time were positioned in a ^{6}Li enriched polyethylene box that provided whole body shielding from the thermal neutrons during an irradiation. The animals' heads were aligned in the middle of a 13 × 2 cm^2 aperture, which served as the beam collimator. Four fission counters, located at the periphery of the 15 cm circular field automatically controlled beam delivery and provided real time data on the relative neutron fluence during an irradiation.

Dosimetry

After completion of BNCT, the animals were held at MIT for ~3 days to allow induced radioactivity to decay before they were returned to The Ohio State University for clinical monitoring. Dosimetric measurements were performed using bare gold foils and a graphite walled ionization chamber (V = 0.1 cm^3) flushed with reagent grade CO_2 on both dead rats and phantoms made from type 6 nylon [44]. The measured dose rates in brain (2.2% nitrogen by weight), normalized to the reactor operating at a power of 5 MW, were 18.5 cGy/min for photons, 7.7 cGy/min for thermal neutrons from the nitrogen capture reaction and 3.4 cGy/min per μg ^{10}B in tissues. For dosimetric calculations, boron concentrations were determined in tumor, normal brain, liver and blood in a separate group of animals 24 h after CED of carboranylporphyrins and 2.5 h after i.v. injection of BPA. Animal irradiations were

performed with the reactor operating at a power between 4.0 and 4.8 MW, and these took approximately 7 min to deliver a thermal neutron fluence of 2.64×10^{12} n.cm^{-2} to complement previous dose prescriptions [45].

Monitoring of clinical status and neuropathologic evaluation

All animals were weighed three times per week and their clinical status was evaluated at the same time. Once the animals had progressively growing tumors, as evidenced by the combination of sustained weight loss, ataxia and peri-orbital hemorrhage, they were euthanized in order to minimize discomfort. Survival times were determined by adding 1 day to the time between tumor implantation and euthanization. The brains of all animals in the therapy studies were removed after death, fixed in 10% buffered formalin, and then cut coronally at the level of the optic chiasm and 2 mm anterior and posterior to it. Tissue sections through the tumor were embedded in paraffin, cut at 4 μm, stained with hematoxylin and eosin (H&E), and examined microscopically to assess the histopathologic changes.

Statistical evaluation

The means and standard deviations (SD) were computed for boron concentrations in all the major organs of C57B1/6 mice bearing s.c. implants of the GL261 murine glioma, as described in Table 1, and for the tumor, brain, and blood of the F98 glioma rats, as described in Table 2. Tumor:-brain and tumor:blood boron concentration ratios were calculated for each group. To study the effects of BNCT on survival of F98 glioma bearing rats, the mean survival time

Table 1 Boron biodistribution in tumor and normal tissue following i.p. injection of either ZnDCP or ZnTCP in mice bearing s.c. implants of the GL261 murine glioma

Agent[a]	Time (h)	Boron concentrations ± SD (μg/g)[b]						Ratios[c]	
		Tumor	Brain	Blood	Liver	Spleen	Muscle	T/Br	T/Bl
ZnDCP	24	8.3 ± 2.7	1.7 ± 0.8	44.5 ± 12.6	94.7 ± 7.3	109.4 ± 10.0	10.9 ± 6.6	4.8	0.2
	48	7.6 ± 1.9	1.2 ± 0.4	15.9 ± 3.5	154.9 ± 28.4	138.5 ± 60.1	6.7 ± 3.2	6.3	0.5
ZnTCP	24	2.0 ± 0.1	0.7 ± 0.6	25.5 ± 31.1	43.1 ± 4.8	115.9 ± 73.6	1.5 ± 0.2	2.6	0.1
	48	5.2 ± 0.3	0.5 ± 0.1	11.3 ± 2.5	46.3 ± 11.5	114.0 ± 99.1	3.0 ± 0.1	10.4	0.5
BPA	2.5	12.5 ± 4.1	1.0 ± 0.2	2.6 ± 0.8	1.1 ± 0.2	3.2 ± 1.9	1.1 ± 0.6	12.5	4.8

[a] ZnDCP or ZnTCP was administered by 3 i.p. injections, administered over 8 h to C57BL/6 mice bearing s.c. implants of the GL261 murine glioma. Animals were euthanized at 24 and 48 h following the third injection and tissues and blood samples were removed for boron determinations. BPA was administered i.p. at a dose of 25 mg b/kg b.w. and mice were euthanized 2.5 h later

[b] Boron concentrations were determined by DCP-AES. The mean boron values (μg/g wt of tissue) ± the standard deviation are shown for groups of four animals

[c] T:Br indicates the tumor to normal brain ratio and T:Bl indicates the tumor to blood ratio

Table 2 Boron biodistribution in F98 glioma bearing rats following administration of escalating doses of H_2TCP by osmotic pumps

Dose (mg/200 μl)	Time (h)	Boron concentration ± SD (μg B/g)[a]			Ratios[b]	
		Tumor	Brain	Blood	T:Br	T:Bl
0.2	0	18.7 ± 8.7	1.3 ± 1.0	0.3 ± 0.3	14.0	64.7
	24	24.6 ± 5.1	2.9 ± 2.7	0.5 ± 0.7	8.5	54.1
	48	9.0 ± 2.7	0.5 ± 0.5	0.3 ± 0.1	18.0	31.9
0.5	0	88.4 ± 20.2	2.0 ± 0.9	0.4 ± 0.2	45.2	207.6
	24	102.9 ± 26.3	3.3 ± 4.1	0.5 ± 0.1	31.3	196.0
	48	16.8 ± 8.4	0.3 ± 0.1	0.3 ± 0.1	49.9	50.5
1.0	0	123.3 ± 61.1	6.5 ± 3.8	0.2 ± 0.1	18.9	593.3
	24	149.6 ± 55.5	10.1 ± 12.6	0.2 ± 0.1	14.8	708.8
	48	34.8 ± 10.8	3.0 ± 1.9	0.3 ± 0.1	11.5	105.5

[a] H_2TCP (0.2–1.0 mg) was administered by means of Alzet osmotic pumps (#2001D) over 24 h to Fischer rats bearing i.c. implants of the F98 glioma. Animals were euthanized at different time point (0, 24, 48 h after termination) and tissues and blood samples were removed for boron determinations by DCP-AES. The values indicated are means ± SD for groups of four to five rats

[b] T:Br indicates the tumor to normal brain ratio of the ipsilateral cerebral hemisphere and T:Bl indicates the tumor to blood ratio

(MST), SD, and median survival time (MeST) were calculated for each group using the Kaplan–Meier estimate [46]. Kaplan–Meier curves also were plotted for all groups. An overall log rank test was performed to test for equality of survival curves over the groups. Wald tests were used for individual comparisons between two groups, with a Bonferroni method of adjustment for multiple comparisons [47]. Since there was no censoring of the survival data, a two sample t test also was used to compare MSTs in order to increase the power of the test. The percent increased life span (% ILS) was determined from the following equation:

$$\%\mathrm{ILS} = \frac{\mathrm{MeST(orMST)_t} - \mathrm{MeST(orMST)_u}}{\mathrm{MeST(orMST)_u}} \times 100$$

where "t" designates treated and "u" designates untreated animals.

Results

Biodistribution after systemic injection of carboranylporphyrins

Following i.p. injection of either ZnDCP or ZnTCP (30 mg B/kg b.w.) to GL261 tumor bearing mice, one of five animals in each group died within the first 24 h and the others demonstrated reduced activity, suggesting that these doses of the zinc complexes were toxic. In contrast, H_2DCP and H_2TCP previously were shown to have very low toxicity [27, 28]. The boron uptake in tumor and normal tissues at 24 and 48 h following the third i.p. injection are summarized in Table 1. The tumor boron concentrations at 48 h were 7.6 ± 1.9 and 5.2 ± 0.3 μg/g of tissue for ZnDCP and ZnTCP, respectively, compared to 1.2 ± 0.4 and 0.5 ± 0.1 μg/g in normal brain. In contrast, the 48 h boron concentrations in the liver were 154.9 ± 28.4 and 46.3 ± 11.5 μg/g, respectively, and the spleen concentrations were 138.5 ± 60.1 and 114.0 ± 99.1 μg/g with marked animal to animal variability. This possibly reflected differences in the excretion of the compounds and their metabolites. The corresponding blood concentrations were 15.9 ± 3.5 and 11.3 ± 2.5 μg/ml, respectively. Based on these data, a decision was made to administer the carboranylporphyrins i.c. either by short term (30 min) CED or by a 24 h infusion using Alzet osmotic pumps. In contrast to the high extracranial tissue uptake of ZnDCP and ZnTCP, BPA had very low concentrations in all organs except for tumor (12.5 ± 4.1 μg/g).

Biodistribution following delivery of carboranylporphyrins by either CED or Alzet pumps

As shown in Tables 2 and 3, administration by either Alzet pumps or CED resulted in higher tumor and lower normal tissue boron concentrations, and improved tumor:brain (T:Br) and tumor:blood (T:Bl) ratios compared to those obtained following i.p. injection (Table 1). The boron concentrations in tumor and selected normal tissues in F98 glioma bearing rats following Alzet pump delivery of H_2TCP at doses of 0.2, 0.5 or 1.0 mg/200 μl, delivered i.c. into F98 glioma bearing rats are summarized in Table 2. Tumor boron concentrations were clearly dose dependent immediately following infusion and at 24 and 48 h later. The highest tumor boron concentrations were observed at 24 h following administration of escalating doses of H_2TCP (24.6, 102.9 and 149.6 μg/g), but these were all within 1 SD of the concentrations that were observed immediately following infusion, indicating that there was retention and possibly some accretion of boron within the tumor. In contrast, the tumor concentrations had fallen

Table 3 Boron concentrations and physical radiation doses delivered in F98 glioma bearing rats 24 h following administration of carboranylporphyrins by osmotic pumps or CED

Agent/route[a]	Boron concentrations (μg/g)[b]			Physical radiation dose[c]		
	Tumor	Brain	Blood	Tumor	Brain	Blood
H_2TCP/pump	102.9 ± 26.3	3.3 ± 4.1	0.7 ± 0.9	25.4	2.5	1.9
H_2TBP/pump	61.9 ± 16.4	0.8 ± 0.9	0.2 ± 0.4	16.0	1.9	1.8
H_2DCP/pump[d]	35.6 ± 9.0	5.2 ± 6.8	0.5 ± 0.5	9.9	2.9	1.9
H_2TBP/CED	140.3 ± 70.9	0.8 ± 0.3	0.2 ± 0.1	34.0	1.9	1.8

[a] H_2DCP, H_2TCD and H_2TBP at doses of 0.5 mg were administered to Fischer rats bearing i.c. implants of the F98 glioma by Alzet osmotic pumps or at a dose of 0.2 mg by CED. The animals were euthanized 24 h after administration and tissues and blood samples were taken for boron determinations

[b] Boron concentrations were determined in samples of tumor, brain, blood, liver, spleen, kidneys, lung and heart, by means of direct current plasma-atomic emission spectroscopy. Except as indicated above, boron concentrations were at the undetectable level (<0.5 μg/g) in all other tissues. The values indicated are means ± standard deviation for groups of four to five rats

[c] Physical dose estimates include contributions from gamma photons, ^{14}N (n,p), ^{14}C and ^{10}B (n,α) ^{7}Li reactions

[d] Based on the low tumor boron values and the calculated physical radiation doses, BNCT was not carried out using H_2DCP

quite precipitously by 48 h to values that were one-third of their peak value, while the normal brain and blood values were low at the three time points (0.2–3.3 μg/g) except for those animals that received the 1.0 mg dose. Their normal brain values were higher at 0, 24 and 48 h (6.5, 10.1 and 3.0 μg/g, respectively). Although the highest T:Br ratio was seen with the dose of 0.5 mg at 48 h after administration, the tumor boron concentration was low (16.8 μg/g). Therefore, the most favorable values of tumor boron (102.9 μg/g) and T:Br ratios for H_2TCP were seen with this dose at 24 h. In contrast, the tumor boron values for H_2TBP and H_2DCP at the same time and dose were 61.9 ± 16.4 and 35.6 ± 9.0 μg/g, respectively (Table 3). The highest tumor boron concentration was seen 24 h following short term (30 min) CED of H_2TBP (140.3 ± 70.9 μg), but as indicated by the large SD, there was considerable animal to animal variability. It should be noted that the T:Br boron concentration ratios of the carboranylporphyrins were markedly increased over those that we have observed following either i.v. or intracarotid (i.c.) administration of BPA and BSH [43].

Boron neutron capture therapy

The carboranylporphyrins were administered 14 days following tumor implantation and BNCT was carried out 24 h after termination of delivery. This was well tolerated and weight loss in the first week was less than 20%, following which the animals regained their weight. The estimated physical radiation doses delivered to tumor, brain and blood were calculated according to boron concentrations summarized in Table 3. In contrast, following i.c. administration of the carboranylporphyrins no boron was detected in samples of liver, spleen, kidneys, lungs and heart (data not shown). The highest physical radiation doses delivered to the tumor were 34.0 Gy for H_2TBP, administered by CED, and 25.4 Gy for H_2TCP, administered by Alzet pumps. The corresponding normal brain doses were 1.9 and 2.5 Gy, respectively (Table 3). The survival data following BNCT are summarized in Table 4, and Kaplan–Meier survival plots are shown in Figs. 2, 3 and 4. The MSTs were 35.0 ± 3.7 and 43.8 ± 10.0 days, respectively, for rats that received H_2TCP and H_2TBP by Alzet pump (Table 4). Animals that received H_2TBP by Alzet pumps had a significantly longer MST than those that received H_2DCP ($P < 0.017$). Further studies were carried out using H_2TBP at a dose of 0.2 mg, administered by CED, either alone or in combination with i.v. BPA. The corresponding MSTs were 33.8 ± 3.1 and 42.8 ± 9.0 days, respectively (Table 4 and Fig. 3). As shown in Fig. 4, there were more long term survivors among rats that received the combination of i.v. BPA and H_2TBP, compared to those that

Table 4 Survival times of F98 glioma bearing rats following i.c. delivery of H_2TCP and H_2TBP by CED or osmotic pumps

Agent/route	Survival time			%ILS[b]	
	N[a]	Range	Mean ± SD	Median	Mean	Median
H_2TCP/pump	18	30–41	35.0 ± 3.7	36	49.6	60.0
H_2TBP/pump	10	32–59	43.8 ± 10.0	40.5	87.2	80.0
H_2TBP/CED	10	30–39	33.8 ± 3.1	33.5	44.4	48.9
H_2TBP/CED + i.v. BPA	9	33–61	42.8 ± 9.0	41	70.0	75.5
BPA/i.v.	10	33–48	39.8 ± 1.6	39.5	59	58
Irradiated controls	9	24–31	27.4 ± 2.7	27	17.3	20.0
Untreated controls	10	21–29	23.4 ± 2.5	22.5	–	–

[a] A total of either 0.2 mg of the compound was administered by CED for 30 min or 0.5 mg by Alzet osmotic pumps for 24 h. BNCT was initiated 24 h after termination of either CED for Alzet osmotic pump infusion or 2.5 h after i.v. administration of BPA

[b] N is the number of animals per group

[c] Percent increased life span (%ILS) was defined relative to the mean and median survival times of untreated controls

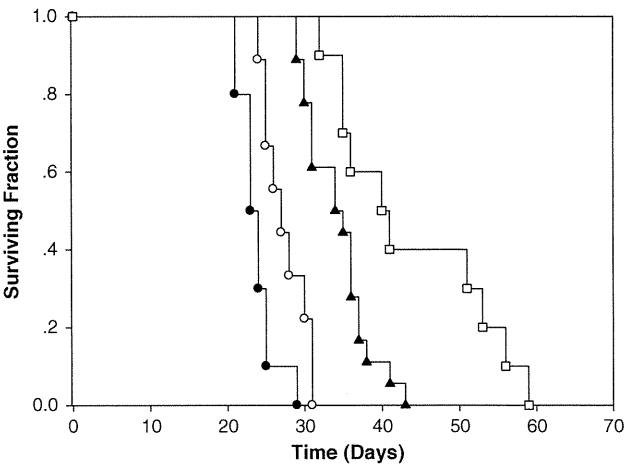

Fig. 2 Kaplan–Meier survival plots for F98 glioma bearing rats following Alzet pump delivery of H_2TCP or H_2TBP followed by BNCT. Survival times in days after implantation have been plotted for untreated animals (*filled circle*), radiation controls (*open circle*), H_2TCP (*filled triangle*) or H_2TBP (*open square*)

received H_2TBP alone ($P < 0.001$). The animals that received of H_2TBP by Alzet pump (Table 4 and Fig. 5) had longer MSTs than those that received it by CED (43.8 vs. 33.8 days), demonstrating that Alzet pump delivery was more effective than CED ($P < 0.013$). If the MSTs of animals that received i.v. BPA are compared to those of rats received H_2TBP by either CED or Alzet pump using a log-rank test, they were not significantly different from one another ($P = 0.38$ and 0.16, respectively). The highest %ILS (87.2%) was observed among those animals that received H_2TBP by osmotic pumps and this was equivalent to the %ILS of animals that received H_2TBP by CED and i.v. BPA (82.8%).

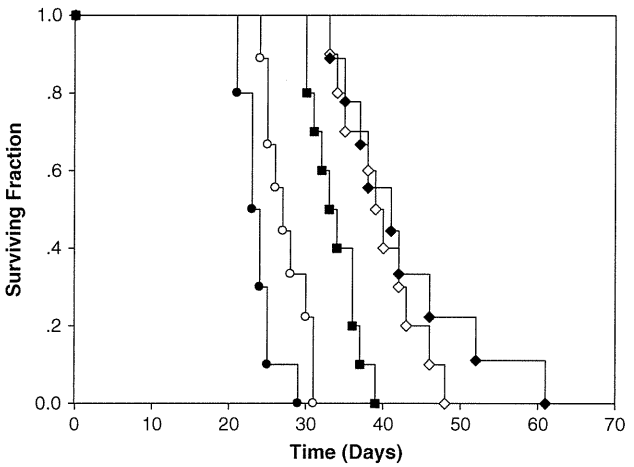

Fig. 3 Kaplan–Meier survival plots for F98 glioma bearing following CED of H_2TBP followed by BNCT. Survival times in days after implantation have been plotted for untreated animals (*filled circle*), irradiation controls (*open circle*), H_2TBP (*filled square*), i.v. BPA (*open diamond*) and H_2TBP plus BPA (*filled diamond*)

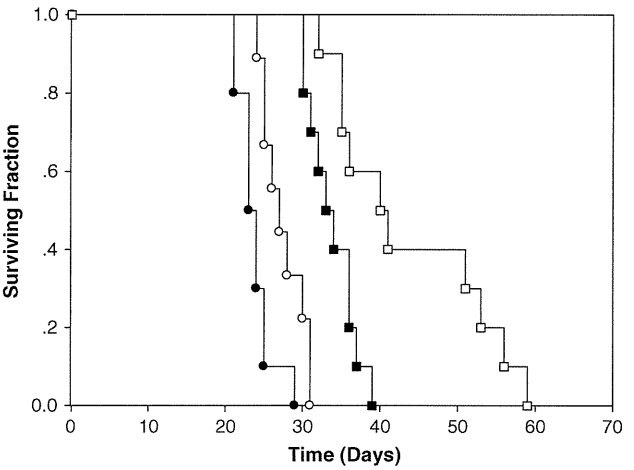

Fig. 4 Kaplan–Meier survival plots for F98 glioma bearing rats following either CED or Alzet pump delivery of H_2TBP followed by BNCT. Survival times in days after implantation have been plotted for untreated animals (*filled circle*), radiation controls (*open circle*), CED delivery of H_2TBP (*filled square*), Alzet pump delivery of H_2TBP (*open square*)

Neuropathologic evaluation

The most notable histopathologic finding was the presence of porphyrin laden macrophages and extracellular deposits of porphyrins in the tumors of many of the rats that received either H_2TCP or H_2TBP by either CED or Alzet pump infusion (Fig. 5A and B). As shown in Fig. 5B, this material was bright orange in color and was easily discernible on H&E stained sections of the tumor. In most instances, the appearance of the tumor in both treated and untreated animals was similar to that previously described by us [39]. As previously described by one of us (RFB), the tumor was composed of cells that varied in size and shape from ovoid to fusiform, sometimes displaying a whorled pattern of growth [42]. Frequently, there were microscopic deposits of tumor cells invading the surrounding white matter and a central zone of necrosis.

Discussion

Biodistribution studies demonstrated that high tumor boron concentrations could be achieved by either short term (30 min) CED or a 24 h infusion via Alzet osmotic pumps. Based on these observations, therapy studies were carried out using H_2TCP and H_2TBP as boron delivery agents. A MST of 43.8 days was obtained using H_2TBP, compared to 35.0 days for H_2TCP, both delivered by Alzet pumps, and 39.8 days for i.v. BPA. Our results are in agreement with those recently reported by Jori et al. [24, 48] who observed that the tumor boron concentrations following i.t. administration of H_2TCP to C57B1/6 mice bearing s.c. implants of the B16 melanoma were 10× greater than those observed following i.v. injection (60 vs. 6 μg/g). However, following BNCT the tumor growth delay was practically identical for both groups. Although the tumor boron concentrations for the latter animals was not determined, published data would suggest that it could have been in the range of 10 μg/g [49]. Similarly, Shibata et al. [50] have reported a very modest increase in the MST of 9L gliosarcoma bearing rats that received a BSH-porphyrin compound designated STA-BX900 (16.2 vs. 14.8 days and 12.8 days for irradiated and untreated control animals, respectively).

However, since the tumor boron concentrations were so much higher following either CED or infusion by Alzet pumps than those obtained with other boron compounds, it was puzzling why the survival data were similar to those obtained with BPA, which had a much lower tumor boron concentration. Histopathologic examination of brains from tumor bearing, BNCT treated rats revealed that in most animals there were large numbers of porphyrin containing macrophages (Fig. 5A and B) indicating that in reality the tumor cell uptake was much lower than would have been predicted, based on the tumor boron values determined by DCP-AES. This provides an explanation as to why the survival data were similar to those obtained with BPA, despite the seemingly high "tumor" boron concentrations. One possible explanation for the high uptake of the carboranylporphyrins by macrophages and the relatively low uptake by tumor cells could be related to their propensity to form aggregates when high concentrations are solubilized in water. This problem could be obviated by initially dissolving them in dimethylsulfoxide (DMSO) and then